PHYSICAL REVIEW D **96,** 014511 (2017)

Extraction of heavy-quark-expansion parameters from unquenched lattice data on pseudoscalar and vector heavy-light meson masses

P. Gambino

Dipartimento di Fisica, Università di Torino and INFN Sezione di Torino, Via P. Giuria 1, I-10125 Torino, Italy

A. Melis

Dep. de Física Teòrica and IFIC, Universitat de València, Dr. Moliner 50, E-46100 Burjassot, Spain

S. Simula

Istituto Nazionale di Fisica Nucleare, Sezione di Roma Tre, Via della Vasca Navale 84, I-00146 Rome, Italy

(Received 2 May 2017; published 25 July 2017)

We present a precise lattice computation of pseudoscalar and vector heavy-light meson masses for heavy-quark masses ranging from the physical charm mass up to ≃4 times the physical b-quark mass. We employ the gauge configurations generated by the European Twisted Mass Collaboration (ETMC) with $N_f = 2 + 1 + 1$ dynamical quarks at three values of the lattice spacing ($a \simeq 0.062, 0.082, 0.089$ fm) with pion masses in the range $M_\pi \simeq 210$–450 MeV. The heavy-quark mass is simulated directly on the lattice up to ≃3 times the physical charm mass. The interpolation to the physical b-quark mass is performed using the ETMC ratio method, based on ratios of the meson masses computed at nearby heavy-quark masses, and adopting the kinetic mass scheme. The extrapolation to the physical pion mass and to the continuum limit yields $m_b^{\rm kin}(1\ {\rm GeV}) = 4.61(20)$ GeV, which corresponds to $\bar{m}_b(\bar{m}_b) = 4.26(18)$ GeV in the $\overline{\rm MS}$ scheme. The lattice data are analyzed in terms of the heavy-quark expansion (HQE) and the matrix elements of dimension-four and dimension-five operators are extracted with a good precision, namely, $\bar{\Lambda} = 0.552(26)$ GeV, $\mu_\pi^2 = 0.321(32)$ GeV^2, and $\mu_G^2(m_b) = 0.253(25)$ GeV^2. The data also allow for a rough estimate of the dimension-six operator matrix elements. As the HQE parameters play a crucial role in the inclusive determination of the Cabibbo-Kobayashi-Maskawa matrix elements V_{ub} and V_{cb}, their precise determination on the lattice may eventually validate and improve the analyses based on fits to the semileptonic moments.

DOI: 10.1103/PhysRevD.96.014511

I. INTRODUCTION

The precise determination of the Cabibbo-Kobayashi-Maskawa (CKM) matrix element V_{cb} is crucial for testing the Standard Model predictions for the rare decays driven by the charged current $b \to c$ transition and in the quest for new physics effects. The information on the CKM entry V_{cb} can be obtained from both inclusive and exclusive semileptonic B-meson decays. In the first case the operator product expansion (OPE) is usually adopted to describe the nonperturbative hadronic physics in terms of a few parameters that can be extracted from experimental data on inclusive $B \to X_c \ell \nu_\ell$ decays together with the CKM element V_{cb} (see, e.g., Refs. [1,2] and references therein). In the second case the relevant hadronic inputs are the semileptonic form factors describing the $B \to D^*(D)\ell\nu_\ell$ decays. The latter are computed using nonperturbative methods, like lattice QCD (LQCD) simulations. As is well known, there is a long-standing tension of about 3 standard deviations between the values of V_{cb} obtained from inclusive or exclusive semileptonic B-meson decays [3], although new evidence suggests that part of this discrepancy may be due to the way the experimental data have been analyzed [4].

The aim of this work is to address the lattice determination of some of the parameters appearing in the OPE analysis of the inclusive B-meson decays. Indeed, the same parameters (or combinations thereof) also appear as coefficients of the heavy-quark expansion (HQE) for the pseudoscalar (PS) and vector (V) heavy-light meson masses. So far, only the charmed and beauty mesons masses, $M_{D^{(*)}}$ and $M_{B^{(*)}}$, could be used to constrain the HQE parameters, and the convergence of the HQE is certainly questionable in the first case. Moreover, only two points are insufficient to determine the coefficients of the HQE for the meson masses with useful precision: they could be pinned down in a much more effective way if one had the meson masses corresponding to heavy quarks with masses between the physical charm and b-quark masses [5], m_c and m_b, or even above m_b. In this work we employ LQCD as a virtual laboratory to compute these meson masses with good accuracy.

We have performed a precise lattice computation of PS and V meson masses for heavy-quark masses ranging from the physical charm mass up to $\simeq$4 times the physical b-quark mass, using the gauge configurations generated by the European Twisted Mass Collaboration (ETMC) with $N_f = 2 + 1 + 1$ dynamical quarks at three values of the lattice spacing ($a \simeq 0.062, 0.082$, and 0.089 fm) and with pion masses in the range $M_\pi \simeq 210$–450 MeV.

Heavy-quark masses are simulated directly on the lattice up to $\simeq$3 times the physical charm mass. The interpolation to the physical b-quark mass is obtained by adopting the *ETMC ratio* method [6], based on ratios of (spin-averaged) meson masses computed at nearby heavy-quark masses. At variance with previous applications of the ETMC ratio method to B physics [6–9], in this work we will adopt the heavy-quark mass defined in the kinetic scheme [10,11] instead of the pole mass. The reason is that the kinetic mass is a short-distance mass free from the main renormalon ambiguities plaguing the pole mass [10–14]. This makes the choice of the kinetic scheme quite attractive for the analysis of inclusive B-meson decay data [15]. The extrapolation to the physical pion mass and to the continuum limit yields $m_b^{\rm kin}(1\ {\rm GeV}) = 4.61(20)$ GeV, which is in agreement with the results of the OPE analysis of the inclusive semileptonic B-meson decays [1,2]. Our result corresponds to $\bar{m}_b(\bar{m}_b) = 4.26(18)$ GeV in the $\overline{\rm MS}$ scheme, which is in agreement with the findings of Ref. [9] as well with other lattice determinations (see, e.g., Ref. [16]).

Then, the ETMC ratio method is applied above the physical b-quark mass to provide heavy-light meson masses towards the static point. The lattice data are analyzed in terms of HQE, taking into account the anomalous dimension and the radiative corrections up to order $\mathcal{O}(\alpha_s^2)$ for the chromomagnetic operator [17–19]. The matrix elements of dimension-four and dimension-five operators, for which radiative corrections are known up to order $\mathcal{O}(\alpha_s^2)$, are extracted with a good precision, namely,

$$\bar{\Lambda} = 0.552(26)\ {\rm GeV}, \tag{1}$$

$$\mu_\pi^2 = 0.321(32)\ {\rm GeV}^2, \tag{2}$$

$$\mu_G^2(m_b) = 0.253(25)\ {\rm GeV}^2. \tag{3}$$

The data also allows to estimate the size of two combinations of the matrix elements of dimension-six operators, for which radiative corrections are not yet available, namely,

$$\rho_D^3 - \rho_{\pi\pi}^3 - \rho_S^3 = 0.153(34)\ {\rm GeV}^3, \tag{4}$$

$$\rho_{\pi G}^3 + \rho_A^3 - \rho_{LS}^3 = -0.158(84)\ {\rm GeV}^3. \tag{5}$$

All of the above HQE parameters, as well as the physical c- and b-quark masses, are highly correlated. Therefore the full covariance matrix is provided (see Tables IV–V). Our results (1)–(5), which are specific to the kinetic scheme, represent the first unquenched lattice determinations of the HQE parameters.

Ours is not the first attempt to extract the HQE parameters from the lattice. In the past, $\bar{\Lambda}$, μ_π^2, and $\mu_G^2(m_b)$ have been estimated using quenched lattice QCD simulations [20–23]. The lattice evaluations of Refs. [21,22] were based on the subtraction of power divergences generated by the mixing of the relevant operators with those of lower dimensionality. Instead, our approach is similar to the one adopted in Ref. [23] and, more recently, in Ref. [24].

The paper is organized as follows. In Sec. II we describe the simulation details. In Sec. III we present the extraction of ground-state PS and V meson masses from the relevant two-point correlators. In Sec. IV we describe the basic features of the ETMC ratio method. In Sec. V we determine the b-quark mass in the kinetic scheme by analyzing the spin-averaged meson masses, while in Sec. VI we analyze the hyperfine mass splitting and determine the mass difference $(M_{B^*} - M_B)$. In Sec. VII we apply the ETMC ratio method to calculate the PS and V meson masses beyond the physical b-quark mass and we perform their analysis in the HQE. Finally, Sec. VIII contains our conclusions.

II. SIMULATION DETAILS

The gauge ensembles used in this work have been generated by ETMC with $N_f = 2 + 1 + 1$ dynamical quarks, which include in the sea (besides two light mass-degenerate quarks) the strange and charm quarks with masses close to their physical values [25,26]. The ensembles are the same as those adopted in Refs. [9,27] to determine the up, down, strange, charm, and bottom-quark masses.

In the ETMC setup the Iwasaki action [28] for the gluons and the Wilson maximally twisted-mass action [29–31] for the sea quarks are employed. Three values of the inverse bare lattice coupling β and different lattice volumes are considered, as shown in Table I, where the number of configurations analyzed (N_{cfg}) corresponds to a separation of 20 trajectories.

At each lattice spacing different values of the light sea-quark mass are considered, and the light valence and sea-quark masses are always taken to be degenerate, i.e., $m_\ell^{\rm sea} = m_\ell^{\rm val} = m_\ell$. In order to avoid the mixing of strange and charm quarks in the valence sector we adopt a nonunitary setup in which the valence strange and charm quarks are regularized as Osterwalder-Seiler fermions [32], while the valence up and down quarks have the same action as the sea. Working at maximal twist, such a setup guarantees an automatic $\mathcal{O}(a)$ improvement [31,33]. Quark masses are renormalized through the renormalization constant (RC) $Z_m = 1/Z_P$, computed nonperturbatively using the RI′-MOM scheme (see Ref. [27]).

TABLE I. Values of the valence-quark bare masses considered for the 15 ETMC gauge ensembles with $N_f = 2 + 1 + 1$ dynamical quarks (see Ref. [27]). $N_{\rm cfg}$ stands for the number of (uncorrelated) gauge configurations used in this work.

ensemble	β	V/a^4	$N_{\rm cfg}$	$a\mu_\ell$	$a\mu_c$	$a\mu_h > a\mu_c$
$A30.32$	1.90	$32^3 \times 64$	150	0.0030	$\{0.21256, 0.25000, 0.29404\}$	$\{0.34583, 0.40675, 0.47840, 0.56267,$
$A40.32$			150	0.0040		$0.66178, 0.77836, 0.91546\}$,
$A50.32$			150	0.0050		
$A40.24$		$24^3 \times 48$	150	0.0040		
$A60.24$			150	0.0060		
$A80.24$			150	0.0080		
$A100.24$			150	0.0100		
$B25.32$	1.95	$32^3 \times 64$	150	0.0025	$\{0.18705, 0.22000, 0.25875\}$	$\{0.30433, 0.35794, 0.42099, 0.49515,$
$B35.32$			150	0.0035		$0.58237, 0.68495, 0.80561\}$
$B55.32$			150	0.0055		
$B75.32$			75	0.0075		
$B85.24$		$24^3 \times 48$	150	0.0085		
$D15.48$	2.10	$48^3 \times 96$	90	0.0015	$\{0.14454, 0.0150, 0.19995\}$	$\{0.23517, 0.27659, 0.32531, 0.38262,$
$D20.48$			90	0.0020		$0.45001, 0.52928, 0.62252\}$
$D30.48$			90	0.0030		

We have considered three values of the valence charm-quark mass, which are needed to interpolate smoothly in the physical charm region. The valence-quark masses are in the following ranges: $3m_{ud}^{\rm phys} \lesssim m_\ell \lesssim 12m_{ud}^{\rm phys}$ and $0.7m_c^{\rm phys} \lesssim m_c \lesssim 1.1m_c^{\rm phys}$. In order to extrapolate up to the b-quark sector we have also considered seven values of the valence heavy-quark mass m_h in the range $1.1m_c^{\rm phys} \lesssim m_h \lesssim 3.3m_c^{\rm phys} \approx 0.8m_b^{\rm phys}$.

The lattice scale is determined using the experimental value of f_{π^+}, while the physical up/down, strange, and charm-quark masses are obtained by using the experimental values for M_π, M_K, and M_{D_s}, respectively [27]. The values of the strange and charm sea-quark masses corresponding to the ETMC ensembles of Table I were calculated in Ref. [27], obtaining a slight mistuning. It was shown that such a mistuning may produce changes in the determination of the physical quark masses that are smaller than other systematic uncertainties.

In Ref. [27] eight branches of the analysis were considered. They differ in:

TABLE II. The input parameters for the eight branches of the analysis of Ref. [27]. The renormalized quark masses and the RC Z_P are given in the $\overline{\rm MS}$ scheme at a renormalization scale of 2 GeV. With respect to Ref. [27] the table includes an update of the values of the lattice spacing and, consequently, of all the other quantities.

	β	1st	2nd	3rd	4th
a^{-1} (GeV)	1.90	2.224(68)	2.192(75)	2.269(86)	2.209(84)
	1.95	2.416(63)	2.381(73)	2.464(85)	2.400(83)
	2.10	3.184(59)	3.137(64)	3.248(75)	3.163(75)
$m_{ud}^{\rm phys}$ (GeV)		0.00372(13)	0.00386(17)	0.00365(10)	0.00375(13)
$m_c^{\rm phys}$ (GeV)		1.183(34)	1.193(28)	1.177(25)	1.219(21)
Z_P	1.90		0.5290(73)		
	1.95		0.5089(34)		
	2.10		0.5161(27)		

	β	5th	6th	7th	8th
a^{-1} (GeV)	1.90	2.222(67)	2.195(75)	2.279(89)	2.219(87)
	1.95	2.414(61)	2.384(73)	2.475(88)	2.411(86)
	2.10	3.181(57)	3.142(64)	3.262(79)	3.177(78)
$m_{ud}^{\rm phys}$ (GeV)		0.00362(12)	0.00377(16)	0.00354(9)	0.00363(12)
$m_c^{\rm phys}$ (GeV)		1.150(35)	1.158(27)	1.144(29)	1.182(19)
Z_P	1.90		0.5730(42)		
	1.95		0.5440(17)		
	2.10		0.5420(10)		

(1) the continuum extrapolation adopting for the scale parameter either the Sommer parameter r_0 or the mass of a fictitious PS meson made up of strange (charm)-like quarks;
(2) the chiral extrapolation performed with fitting functions chosen to be either a polynomial expansion or a chiral perturbation theory ansatz in the light-quark mass;
(3) the choice between the methods M1 and M2, which differ by $O(a^2)$ effects, used to determine the mass RC $Z_m = 1/Z_P$ in the RI'-MOM scheme.

In the present analysis we make use of the input parameters corresponding to each of the eight branches of Ref. [27]. The central values and the errors of the input parameters, evaluated using bootstrap samplings with $\mathcal{O}(100)$ events, are collected in Table II. Throughout this work all of the results obtained within the above branches are averaged according to Eq. (28) of Ref. [27].

III. EXTRACTION OF GROUND-STATE MESON MASSES

The ground-state mass of PS and V mesons can be determined by studying the appropriate two-point correlation functions at large (Euclidean) time distances t from the source, viz.,

$$C_{\rm PS}(t) = \left\langle \sum_{\vec{x}} P_5(\vec{x},t) P_5^\dagger(0,0) \right\rangle \underset{t\geq t_{\rm min}^{\rm PS}}{\longrightarrow} \frac{Z_{\rm PS}}{2M_{\rm PS}} \times \left[e^{-M_{\rm PS}t} + e^{-M_{\rm PS}(T-t)}\right], \tag{6}$$

$$C_{\rm V}(t) = \frac{1}{3}\left\langle \sum_{i,\vec{x}} V_i(\vec{x},t) V_i^\dagger(0,0) \right\rangle \underset{t\geq t_{\rm min}^{\rm V}}{\longrightarrow} \frac{Z_{\rm V}}{2M_{\rm V}} \times \left[e^{-M_{\rm V}t} + e^{-M_{\rm V}(T-t)}\right], \tag{7}$$

where $M_{\rm PS(V)}$ is the PS(V) ground-state mass and $t_{\rm min}^{\rm PS(V)}$ stands for the minimum time distance at which the PS(V) ground state can be considered well isolated. In Eqs. (6)–(7), $V_i(x) = \bar{q}_1(x)\gamma_i q_2(x)$ and $P_5(x) = \bar{q}_1(x)\gamma_5 q_2(x)$ represent, respectively, the interpolating fields for V and PS mesons, made of two valence quarks q_1 and q_2 with bare masses μ_1 and μ_2. We set opposite values for the Wilson parameters of the two valence quarks ($r_1 = -r_2$), because this choice guarantees that the cutoff effects on the PS mass are $\mathcal{O}[a^2(\mu_1+\mu_2)]$ [31]. In what follows we will consider the quark q_1 to be either in the charm region or above, i.e., $q_1 = c, h$, while the quark q_2 is always taken to be a light quark with bare mass μ_ℓ (see Table I).

The PS(V) ground-state mass, $M_{\rm PS(V)}$, can be determined from the plateau of the effective mass $M_{\rm PS(V)}^{\rm eff}(t)$ at large time distances, viz.,

$$M_{\rm PS(V)}^{\rm eff}(t) \equiv \operatorname{arcosh}\left[\frac{C_{\rm PS(V)}(t-1) + C_{\rm PS(V)}(t+1)}{2C_{\rm PS(V)}(t)}\right] \underset{t\geq t_{\rm min}^{\rm PS(V)}}{\longrightarrow} M_{\rm PS(V)}. \tag{8}$$

The statistical accuracy of the meson correlators (6)–(7) can be significantly improved by the use of the "one-end" trick stochastic method [34,35], which employs spatial stochastic sources at a single time slice chosen randomly. Besides the use of local interpolating quark fields, in the case of charm or heavier quarks it is also a common procedure to adopt Gaussian-smeared interpolating quark fields [36] in order to suppress the contribution of the excited states more quickly, leading to an improved projection onto the ground state at relatively small time distances. For the values of the smearing parameters, we set $k_G = 4$ and $N_G = 30$. In addition, we apply APE smearing

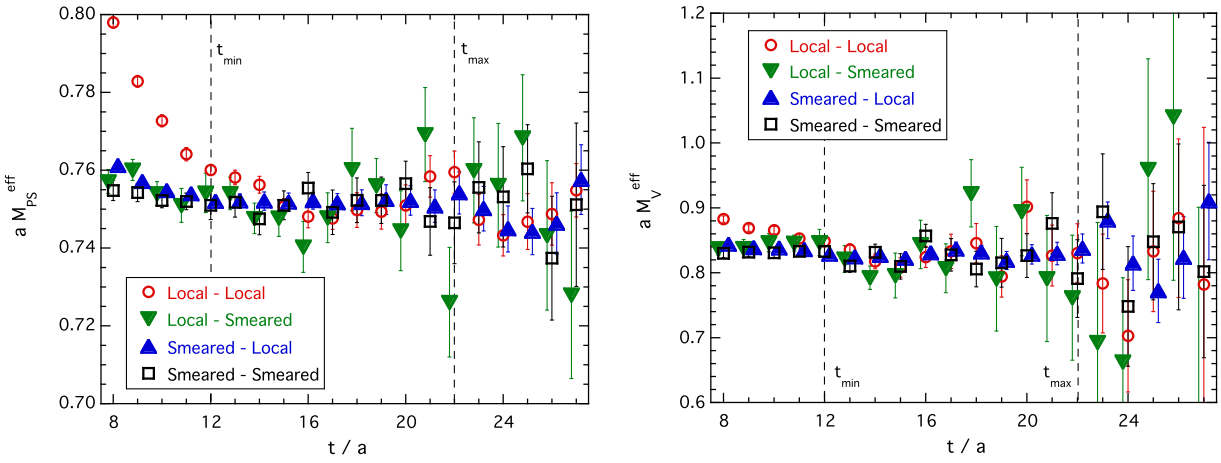

FIG. 1. Left panel: Effective masses of the four correlators $C_{\rm PS}^{LL}(t)$, $C_{\rm PS}^{LS}(t)$, $C_{\rm PS}^{SL}(t)$, and $C_{\rm PS}^{SS}(t)$, calculated for a $(c\ell)$ meson using Eq. (8) in the case of the ETMC gauge ensemble B55.32 (corresponding to a pion mass $\simeq$380 MeV). Right panel: The same as in the left panel, but for the vector correlators $C_{\rm V}^{LL}(t)$, $C_{\rm V}^{LS}(t)$, $C_{\rm V}^{SL}(t)$, and $C_{\rm V}^{SS}(t)$.

TABLE III. Values of $t_{\rm min} = t^{\rm PS}_{\rm min} = t^{V}_{\rm min}$, $t^{\rm PS}_{\rm max}$, and $t^{V}_{\rm max}$ chosen to extract the ground-state signal from the effective mass (8), evaluated for heavy-light mesons with valence-quark content ($c\ell$), using the SL correlators (i.e, smeared quark fields in the source and local ones in the sink) in the case of the ETMC gauge ensembles of Table I.

β	V/a^4	$t_{\rm min}/a$	$t^{\rm PS}_{\rm max}/a$	$t^{V}_{\rm max}/a$
1.90	$32^3 \times 64$	10	30	20
	$24^3 \times 48$	10	20	18
1.95	$32^3 \times 64$	12	22	20
	$24^3 \times 48$	12	20	18
2.10	$48^3 \times 96$	16	44	36

to the gauge links [37] in the interpolating fields with parameters $\alpha_{\rm APE} = 0.5$ and $N_{\rm APE} = 20$.

We have implemented smeared fields both in the source and in the sink. We have therefore evaluated two-point correlation functions corresponding to the four possible combinations generated by using local/smeared fields at the source/sink, namely, $C^{LL}_{\rm PS(V)}(t)$, $C^{LS}_{\rm PS(V)}(t)$, $C^{SL}_{\rm PS(V)}(t)$, and $C^{SS}_{\rm PS(V)}(t)$, where L and S denote local and smeared operators, respectively.

For the whole set of charm and heavier quark masses shown in Table I, the SL correlation functions exhibit the best signal-to-noise ratio, as illustrated in Fig. 1 for a ($c\ell$) meson in the case of the gauge ensemble B55.32.

Thus, the SL correlators have been used to extract the ground-state masses from the plateau of the effective mass (8) in the range $t^{\rm PS(V)}_{\rm min} \le t \le t^{\rm PS(V)}_{\rm max}$. The stability of the extracted ground-state masses with respect to changes of both $t^{\rm PS(V)}_{\rm min}$ and $t^{\rm PS(V)}_{\rm max}$ has been studied and our choices for the values of $t^{\rm PS}_{\rm min} = t^{V}_{\rm min} = t_{\rm min}$, $t^{\rm PS}_{\rm max}$, and $t^{V}_{\rm max}$ in the charm sector are given in Table III.

The quality of the plateaux of the effective mass (8) is illustrated in Fig. 2 for a series of both PS and V heavy-light ($h\ell$) mesons in the case of the gauge ensemble A40.32. It can be seen that the higher the heavy-quark mass, the smaller the value adopted for $t_{\rm max}$, while the value chosen for $t_{\rm min}$ is independent of the heavy-quark mass.

We have checked our determination of the ground-state masses $M_{\rm PS(V)}$ by employing an alternative method, namely, the generalized eigenvalue problem (GEVP) method of Ref. [38], which is based on the simultaneous use of the four correlators $C^{LL}_{\rm PS(V)}(t)$, $C^{LS}_{\rm PS(V)}(t)$, $C^{SL}_{\rm PS(V)}(t)$, and $C^{SS}_{\rm PS(V)}(t)$. It turns out that the GEVP method provides ground-state masses that are in nice agreement with those determined directly from the effective mass of the SL correlators with a slightly larger uncertainty. Finally, we have also checked that the impact of increasing by two units the values adopted for $t_{\rm min}$ in Table III on the extracted PS and vector-meson masses is negligible within present statistical uncertainties.

IV. THE ETMC RATIO METHOD

Since the lattice spacing of the ETMC gauge ensembles does not allow to directly simulate a b quark on the lattice, the determination of quantities in the beauty sector requires alternative strategies. In this respect a very suitable method is represented by the ETMC ratio method, which has already been applied in the $N_f = 2$ framework [6–8] as well as in the $N_f = 2 + 1 + 1$ case [9] to determine the mass of the b quark, the leptonic decay constants, and the bag parameters of $B_{(s)}$ mesons.

The ETMC ratio method consists of three main steps. The first one is the calculation of the observable of interest at heavy-quark masses around the charm scale, for which relativistic simulations are reliable with well-controlled discretization errors. In the second step, appropriate ratios

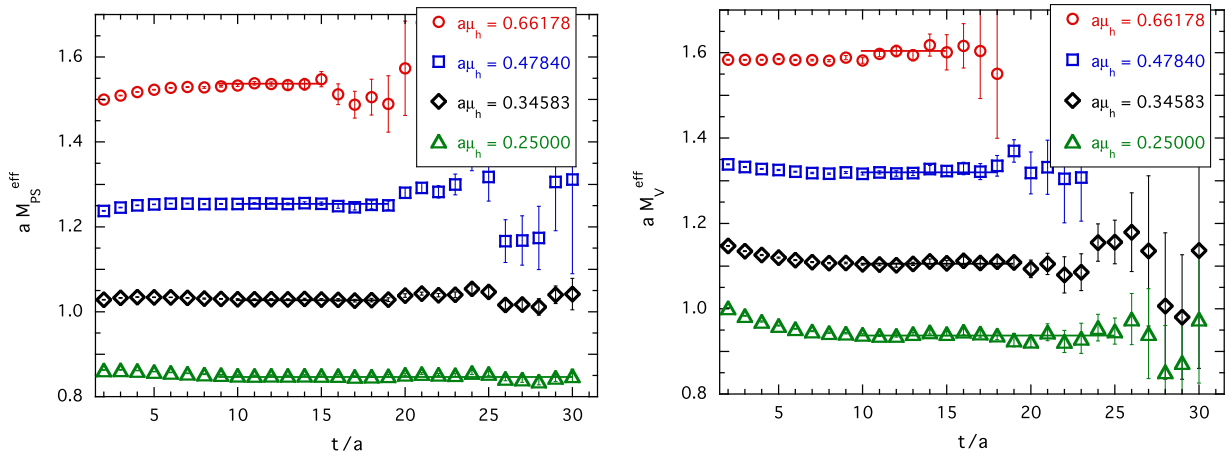

FIG. 2. Left panel: Effective masses of the correlator $C^{SL}_{\rm PS}(t)$ calculated for various ($h\ell$) mesons using Eq. (8) in the case of the ETMC gauge ensemble A40.32 (corresponding to a pion mass ≃320 MeV). Right panel: The same as in the left panel, but for the vector correlator $C^{SL}_{\rm V}(t)$. The solid lines identify the plateau region $t_{\rm min} \le t \le t_{\rm max}$ selected for each value of the heavy-quark mass.

of the observable are evaluated at increasing values of the heavy-quark mass up to a scale ≈3 times the charm-quark mass (i.e., around 3 GeV). The crucial point is that the static limit of the ratios is exactly known from heavy-quark effective theory (HQET) arguments. The final step of the computation is a smooth interpolation of the lattice data from the charm region to the infinite mass point, so that the value of the observable at the b-quark or B-meson mass can be determined.

The great computational advantage of the ratio method is that B-physics computations can be carried out using the same relativistic action setup with which the lighter quark computations are performed. Moreover, an extra simulation at the static point limit is not necessary, while the exact information about it is automatically incorporated in the construction of the ratios of the observable. It should also be stressed that the use of ratios greatly helps in reducing the discretization errors.

As already explained in the Introduction, we are interested in studying the heavy-quark mass dependence of the following meson mass combinations:

$$M_{av}(\tilde{m}_h) \equiv \frac{M_{\rm PS}(\tilde{m}_h) + 3M_{\rm V}(\tilde{m}_h)}{4}, \tag{9}$$

$$\Delta M(\tilde{m}_h) \equiv M_{\rm V}(\tilde{m}_h) - M_{\rm PS}(\tilde{m}_h), \tag{10}$$

where $\tilde{m}_h = m_h^{\rm kin}(\mu_{\rm soft})$ is the renormalized heavy-quark mass in the kinetic scheme [11] at a soft cutoff $\mu_{\rm soft}$, which is chosen to be equal to $\mu_{\rm soft} = 1$ GeV. For the sake of clarity, in what follows the renormalized quark mass in the $\overline{\rm MS}$ scheme at a renormalization scale μ will be denoted by $\bar{m}_h(\mu)$.

At variance with previous applications of the ETMC ratio method, in this work we will adopt the heavy-quark mass $\tilde{m}_h$ defined in the kinetic scheme instead of the pole mass $m_h^{\rm pole}$. The main reason is that the relation between the pole mass and the bare lattice masses μ_h suffers in perturbation theory from infrared renormalon ambiguities of order $O(\Lambda_{\rm QCD})$ [10–14]. By the same token, the HQE parameter $\bar{\Lambda}$—which measures the difference between the heavy-hadron and heavy-quark masses—is also affected by renormalon uncertainties, and the same applies to other HQE parameters. The kinetic mass $\tilde{m}_h$ offers a solution to the above problem by subtracting the infrared sensitive part from the pole mass [11,39], leading to a short-distance mass and to HQE parameters free from renormalon ambiguities.

The relation between the simulated bare heavy-quark mass $a\mu_h$ (see Table I) and the kinetic mass $\tilde{m}_h$ can be obtained in three steps. First, using the values of the lattice spacing and of the RC Z_P from Table II, one gets

$$\bar{m}_h(2\ {\rm GeV}) = \frac{1}{Z_P a}(a\mu_h). \tag{11}$$

Then, the perturbative scale can be evolved from $\mu = 2$ GeV to the value $\mu = \bar{m}_h$ using next-to-next-to-next-to-leading-order perturbation theory [40] with four quark flavors ($n_\ell = 4$) and $\Lambda_{\rm QCD}^{Nf=4} = 297(8)$ MeV [3], obtaining in this way $\bar{m}_h(\bar{m}_h)$. Finally, the relation between the kinetic mass $\tilde{m}_h$ and the $\overline{\rm MS}$ mass $\bar{m}_h(\bar{m}_h)$ is known up to two loops [15], namely,

$$\begin{aligned}\tilde{m}_h = \bar{m}_h(\bar{m}_h)\Bigg\{1 &+ \frac{4}{3}\frac{\alpha_s(\bar{m}_h)}{\pi}\left[1 - \frac{4}{3}x - \frac{1}{2}x^2\right] + \left(\frac{\alpha_s(\bar{m}_h)}{\pi}\right)^2 \\ &\cdot\Bigg[\frac{\beta_0}{24}(8\pi^2+71) + \frac{35}{24} + \frac{\pi^2}{9}\ln(2) - \frac{7\pi^2}{12} - \frac{\zeta_3}{6} \\ &+ \frac{4}{27}x(24\beta_0\ln(2x) - 64\beta_0 + 6\pi^2 - 39) \\ &+ \frac{1}{18}x^2(24\beta_0\ln(2x) - 52\beta_0 + 6\pi^2 - 23) \\ &- \frac{32}{27}x^3 - \frac{4}{9}x^4\Bigg] + \mathcal{O}(\alpha_s^3)\Bigg\},\end{aligned} \tag{12}$$

where $x \equiv \mu_{\rm soft}/\bar{m}_h(\bar{m}_h)$, $\beta_0 = (33 - 2n_\ell)/12$, and $\zeta_3 \simeq 1.20206$. We remind the reader that in the limit $\mu_{\rm soft} \to 0$ the kinetic mass $\tilde{m}_h$ coincides with the heavy-quark pole mass $m_h^{\rm pole}$. Between the charm and bottom scales the ratio $\tilde{m}_h/\bar{m}_h(\bar{m}_h)$ varies in the range 0.8–1.1 and may be subject to important higher-order corrections. In Sec. VII we will take into account the ensuing theoretical uncertainty. Even within the present $\mathcal{O}(\alpha_s^2)$ accuracy the uncertainty in the determination of $\tilde{m}_h$ can be decreased by optimizing the choice of the $\overline{\rm MS}$ scale in Eq. (11): we leave this for future improvements.

V. DETERMINATION OF THE b-QUARK MASS

We start by applying the ratio method to the quantity $M_{av}(\tilde{m}_h)$ [see Eq. (9)]. To this end we construct a sequence of heavy-quark masses $\tilde{m}_h^{(n)}$ such that every two successive quark masses have a common fixed ratio λ, i.e., for $n = 2, 3, \ldots$

$$\tilde{m}_h^{(n)} = \lambda \tilde{m}_h^{(n-1)}. \tag{13}$$

The series of masses starts at the physical charm-quark mass $\tilde{m}_h^{(1)} = \tilde{m}_c = 1.219(41)$ GeV corresponding to the result $\bar{m}_c(2\ {\rm GeV}) = 1.176(36)$ GeV obtained in Ref. [27] using the experimental mass of the D_s meson. For each gauge ensemble the quantity $M_{av}(\tilde{m}_c)$ can be safely computed by a smooth interpolation of the results corresponding to the subset of the bare-quark masses in the charm region (see $a\mu_c$ in Table I). The lattice data for $M_{av}(\tilde{m}_c)$ depend on the (renormalized) light-quark mass $\bar{m}_\ell$ and on the lattice spacing a. They can be safely extrapolated to the physical pion mass (see $m_{ud}^{\rm phys}$ in Table II) and to the continuum limit using a simple, combined linear fit in both $\bar{m}_\ell$ and a^2 [thanks to the

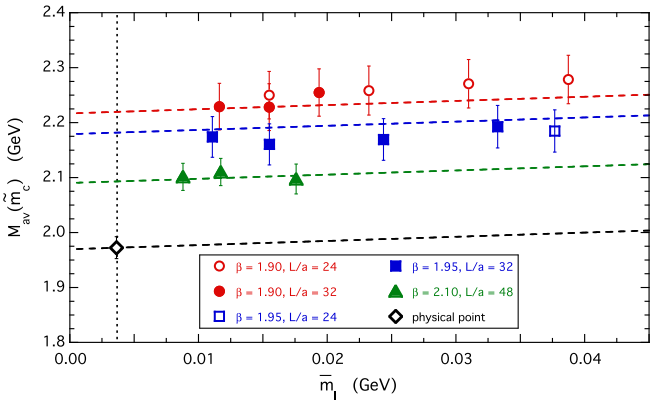

FIG. 3. The quantity $M_{av}(\tilde{m}_h^{(1)}) = M_{av}(\tilde{m}_c)$ versus the (renormalized) light-quark mass $\bar{m}_\ell = \bar{m}_\ell(2\ \mathrm{GeV})$ for the various ETMC gauge ensembles. The dashed lines are the results of a linear fit in both $\bar{m}_\ell$ and a^2 at each value of the lattice spacing and in the continuum limit. The diamond is the result at the physical light-quark mass m_{ud}^{phys} (see Table II) in the continuum limit.

automatic $\mathcal{O}(a)$ improvement of our lattice setup], as shown in Fig. 3. At the physical pion mass in the continuum limit we get $M_{av}^{\mathrm{phys}}(\tilde{m}_c) = 1.967(25)$ GeV, which agrees with the experimental value $(M_D + 3M_{D^*})/4 = 1.973$ GeV from the Particle Data Group (PDG) [3] as well as with the result $M_{av}^{\mathrm{phys}}(\tilde{m}_c) = 1.975(11)$ GeV based on the direct investigation of the D^*- to D-meson mass ratio of Ref. [41].

Analogously, for each gauge ensemble the quantities $M_{av}(\tilde{m}_h^{(n)})$ with $n = 2, 3, \ldots$ can be evaluated by interpolating the results corresponding to the subset of the bare heavy-quark masses (see $a\mu_h$ in Table I).

Then, we construct the following ratios:

$$y_M(\tilde{m}_h^{(n)}, \lambda) = \frac{M_{av}(\tilde{m}_h^{(n)})}{M_{av}(\tilde{m}_h^{(n-1)})} \frac{\tilde{m}_h^{(n-1)}}{\tilde{m}_h^{(n)}} = \lambda^{-1} \frac{M_{av}(\tilde{m}_h^{(n)})}{M_{av}(\tilde{m}_h^{(n-1)})}, \tag{14}$$

with $n = 2, 3, \ldots$. The advantage of considering the ratios (14) is that the discretization effects affecting the spin-averaged meson masses $M_{av}(\tilde{m}_h^{(n)})$ and $M_{av}(\tilde{m}_h^{(n-1)})$ are typically above 10%, but they largely compensate in the ratios (14) even at the largest values of the heavy-quark mass. This is nicely illustrated in Fig. 4, where the difference between the continuum results (black dashed lines) and those obtained at the finest lattice spacing (green dashed lines) differ by less than 1% both at intermediate values of $\tilde{m}_h$ (left panel) and at the highest values of $\tilde{m}_h$ (right panel).

Each of the ratios $y_M(\tilde{m}_h^{(n)}, \lambda)$ is therefore extrapolated to the physical pion mass and to the continuum limit using again a combined linear fit in both $\bar{m}_\ell$ and a^2, obtaining a value which will be denoted hereafter by $\bar{y}_M(\tilde{m}_h^{(n)}, \lambda)$. We have checked the possible impact of a few systematics in the chiral and continuum limit extrapolations by considering either the inclusion of a quadratic term in the light-quark mass or the exclusion of the data at the coarsest lattice spacing ($\beta = 1.90$). In both cases the differences of the extrapolated values $\bar{y}_M(\tilde{m}_h^{(n)}, \lambda)$ are within the statistical uncertainties.

In the static limit $\tilde{m}_h \to \infty$ the HQE predicts

$$\lim_{\tilde{m}_h \to \infty} \frac{M_{av}(\tilde{m}_h)}{\tilde{m}_h} = 1, \tag{15}$$

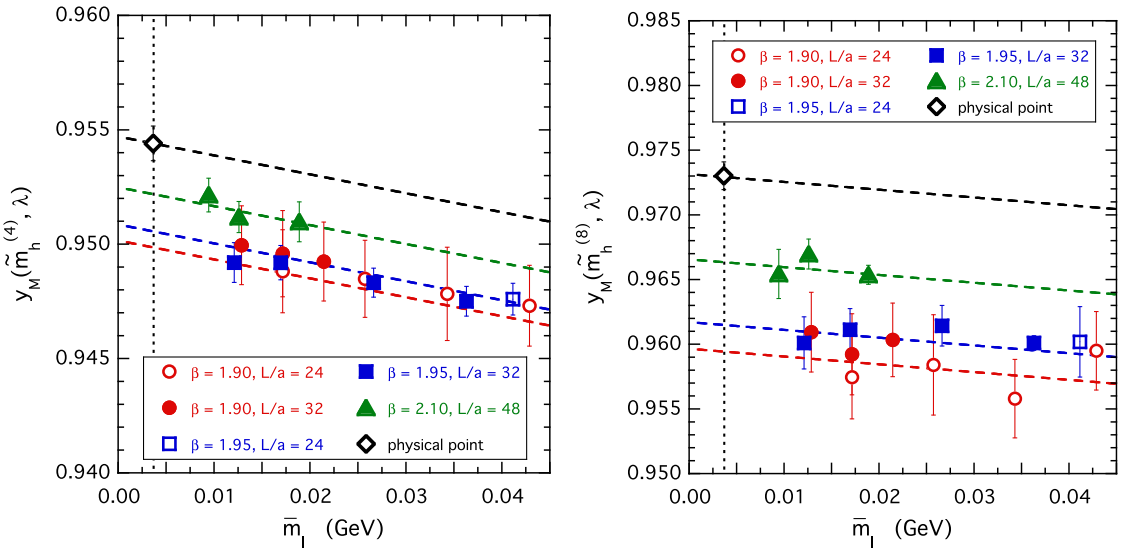

FIG. 4. The ratios $y_M(\tilde{m}_h^{(4)}, \lambda)$ (left panel) and $y_M(\tilde{m}_h^{(8)}, \lambda)$ (right panel) versus the (renormalized) light-quark mass $\bar{m}_\ell = \bar{m}_\ell(2\ \mathrm{GeV})$ for the various ETMC gauge ensembles. The dashed lines are the results of a linear fit in both $\bar{m}_\ell$ and a^2. The diamonds correspond to the values $\bar{y}_M(\tilde{m}_h^{(4)}, \lambda)$ and $\bar{y}_M(\tilde{m}_h^{(8)}, \lambda)$, obtained at the physical light-quark mass m_{ud}^{phys} (see Table II) in the continuum limit.

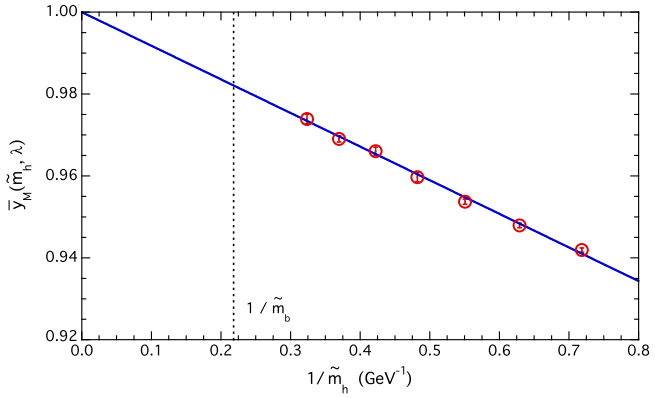

FIG. 5. Lattice data for the ratio $\bar{y}_M(\tilde{m}_h, \lambda)$ versus the inverse heavy-quark mass $1/\tilde{m}_h$. The solid line is the result of the HQE-constrained fit (16) with $\epsilon_2 = 0$, taking into account the correlation matrix among the lattice points. The vertical dotted line corresponds to the position of the inverse physical b-quark mass $1/\tilde{m}_b$.

which implies $\lim_{\tilde{m}_h \to \infty} \bar{y}_M(\tilde{m}_h, \lambda) = 1$ for any value of λ. Thus the $\tilde{m}_h$ dependence of $\bar{y}_M$ can be described as a series expansion in terms of $1/\tilde{m}_h$, namely,

$$\bar{y}_M(\tilde{m}_h, \lambda) = 1 + \frac{\epsilon_1}{\tilde{m}_h} + \frac{\epsilon_2}{\tilde{m}_h^2} + \mathcal{O}\left(\frac{1}{\tilde{m}_h^3}\right), \tag{16}$$

where the coefficients $\epsilon_{1,2}$ may depend upon λ. The lattice data for the ratio $\bar{y}_M(\tilde{m}_h, \lambda)$ are shown in Fig. 5 as a function of the inverse heavy-quark mass $1/\tilde{m}_h$. It can be seen that a linear fit, i.e., Eq. (16) with $\epsilon_2 = 0$, is sufficient to fit the data when taking into account the correlations between the lattice points. For each of the eight branches of the analysis (see Table II) the correlation matrix is constructed and the corresponding correlated χ^2 variable is minimized. The quality of the fit (16) with $\epsilon_2 = 0$ is illustrated in Fig. 5.

Finally, the chain equation

$$\bar{y}_M(\tilde{m}_h^{(2)}, \lambda)\bar{y}_M(\tilde{m}_h^{(3)}, \lambda)\ldots\bar{y}_M(\tilde{m}_h^{(K+1)}, \lambda) = \lambda^K \frac{M_{av}\left(\tilde{m}_h^{(K+1)}\right)}{M_{av}(\tilde{m}_c)}, \tag{17}$$

in which the various factors in the lhs are evaluated through the fitting function (16), allows to determine the b-quark mass $\tilde{m}_b$ by requiring that after K (integer) steps the quantity $M_{av}(\tilde{m}_h^{(K+1)})$ matches the experimental value $(M_B + 3M_{B^*})/4 = 5.314$ GeV [3]. Then the b-quark mass $\tilde{m}_b$ is directly given by $\tilde{m}_b = \lambda^K \tilde{m}_c$. In practice an iterative procedure should be applied in order to tune the value of the parameter λ once the value of the integer K is chosen. Adopting $K = 10$, we find $\lambda = 1.1422(10)$, which yields

$$\tilde{m}_b = 4.605(120)_{\rm stat}(57)_{\rm syst}\ \text{GeV} = 4.605(132)\ \text{GeV}, \tag{18}$$

where the systematic error comes from the eight branches of the input parameters of Table II. Translated into the $\overline{\rm MS}$ scheme, the result (18) corresponds to $\bar{m}_b(\bar{m}_b) = 4.257\ (108)_{\rm stat}\ (52)_{\rm syst}$ GeV $= 4.257\ (120)$ GeV, which is well compatible with the ETMC determination $\bar{m}_b(\bar{m}_b) = 4.26\ (10)$ GeV given in Ref. [9] and consistent with other lattice determinations within 1 standard deviation (see, e.g., the FLAG review [16]). The analysis of Ref. [9] shares the same ETMC gauge ensembles, but it differs in i) the use of the heavy-quark running mass $\bar{m}_h\ (2\text{GeV})$ instead of the kinetic mass $\tilde{m}_h$, ii) a different definition of the ratios (14), and iii) the use of the experimental values of B- and B_s-meson masses instead of the spin-averaged B-meson mass to determine the b-quark mass.

Before closing this section we note that the correlation ρ between the determination (18) and the input value of the charm mass is 100%, viz.,

$$\rho[\tilde{m}_b, \tilde{m}_c] = +1. \tag{19}$$

We expect that such a strong correlation will play a role in the extraction of the CKM element $|V_{cb}|$ from inclusive semileptonic B-meson decays. Indeed, up to now in the OPE treatment of inclusive data the charm and bottom-quark masses have been considered as uncorrelated parameters.

VI. ANALYSIS OF THE HYPERFINE MESON MASS SPLITTING

In this section we apply the ratio method to the hyperfine meson mass splitting $\Delta M(\tilde{m}_h)$ [see Eq. (10)].

As in the case of the spin-averaged meson mass $M_{av}(\tilde{m}_c)$, for each gauge ensemble the quantity $\Delta M(\tilde{m}_c)$ at the triggering point $\tilde{m}_c$ is computed by interpolating the results corresponding to the subset of the bare-quark masses in the charm region (see $a\mu_c$ in Table I). Then the lattice data for $\Delta M_{av}(\tilde{m}_c)$ are safely extrapolated to the physical pion mass and to the continuum limit using a combined linear fit in both $\bar{m}_\ell$ and a^2, as illustrated in Fig. 6.

At the physical pion mass in the continuum limit we get $\Delta M^{\rm phys}(\tilde{m}_c) = 140(11)$ MeV, which nicely agrees with the experimental value $M_{D^*} - M_D = 141.4$ MeV from PDG [3] as well as with the result $M_{D^*} - M_D = 144(15)$ MeV obtained in Ref. [41] from a direct investigation of the D^*- to D-meson mass ratio.

Analogously, for each gauge ensemble the quantities $\Delta M(\tilde{m}_h^{(n)})$ with $n = 2, 3, \ldots$ are evaluated by interpolating the results corresponding to the subset of the bare heavy-quark masses (see $a\mu_h$ in Table I). We now consider the following ratios:

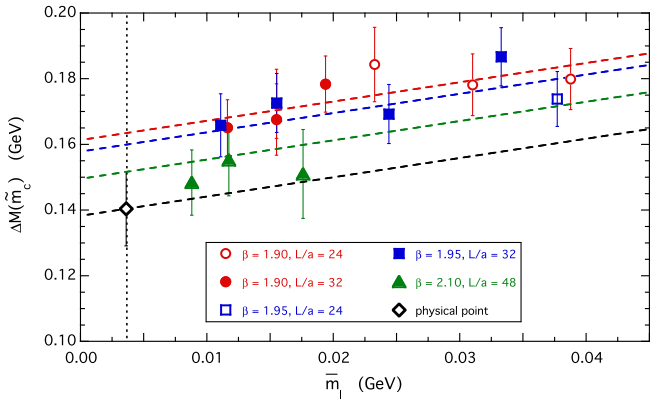

FIG. 6. The quantity $\Delta M(\tilde{m}_h^{(1)}) = \Delta M(\tilde{m}_c)$ versus the (renormalized) light-quark mass $\bar{m}_\ell = \bar{m}_\ell(2\ \mathrm{GeV})$ for the various ETMC gauge ensembles. The dashed lines are the results of a linear fit in both $\bar{m}_\ell$ and a^2 at each value of the lattice spacing and in the continuum limit. The black diamond is the result at the physical light-quark mass m_{ud}^{phys} (see Table II) in the continuum limit.

$$y_{\Delta M}(\tilde{m}_h^{(n)}, \lambda) \equiv \frac{\tilde{m}_h^{(n)}}{\tilde{m}_h^{(n-1)}} \frac{\Delta M(\tilde{m}_h^{(n)})}{\Delta M(\tilde{m}_h^{(n-1)})} \frac{c_G(\tilde{m}_h^{(n-1)}, \tilde{m}_b)}{c_G(\tilde{m}_h^{(n)}, \tilde{m}_b)} = \lambda \frac{\Delta M(\tilde{m}_h^{(n)})}{\Delta M(\tilde{m}_h^{(n-1)})} \frac{c_G(\tilde{m}_h^{(n-1)}, \tilde{m}_b)}{c_G(\tilde{m}_h^{(n)}, \tilde{m}_b)}, \tag{20}$$

where $c_G(\tilde{m}_h, \tilde{m}_b)$ is the short-distance Wilson coefficient that multiplies the matrix element of the HQET chromomagnetic operator renormalized in the $\overline{\mathrm{MS}}$ scheme at the scale of the physical b-quark mass through a multiplicative RC, $Z_{\mathrm{CMO}}(\bar{m}_b)$, viz.,

$$\mu_G^2(\bar{m}_b) \equiv Z_{\mathrm{CMO}}(\bar{m}_b) \frac{\langle B|\bar{h}_v G_{\mu\nu}\sigma^{\mu\nu} h_v|B\rangle}{2\langle B|B\rangle}, \tag{21}$$

with h_v being the field describing a heavy quark inside a hadron moving with velocity v. Note that the ratio (20) is independent of the reference scale of the physical b-quark mass [see Eq. (24)].

The coefficient c_G is given by the product of three factors,

$$c_G = \bar{c}_G \cdot \mathcal{R} \cdot \frac{\tilde{m}_h}{m_h^{\mathrm{pole}}}, \tag{22}$$

where $\bar{c}_G$ matches the HQE chromomagnetic operator with the corresponding one in QCD, $\mathcal{R}$ represents its running in the $\overline{\mathrm{MS}}$ scheme, and the factor $\tilde{m}_h/m_h^{\mathrm{pole}}$ is introduced to cancel the pole mass from the contribution of the chromomagnetic operator to the hyperfine splitting, improving in this way the convergence of the perturbative expansion. An alternative method to achieve this was presented in Refs. [17,18].

The conversion coefficient $\bar{c}_G$ is known up to three loops in terms of $\alpha_s(m_h^{\mathrm{pole}})$ [19]. At two loops and in terms of $\alpha_s(\bar{m}_h)$ one gets

$$\bar{c}_G = 1 + \frac{13}{6}\frac{\alpha_s(\bar{m}_h)}{\pi} + (11.4744\beta_0 - 9.6584)\left(\frac{\alpha_s(\bar{m}_h)}{\pi}\right)^2 + \mathcal{O}(\alpha_s^3). \tag{23}$$

The evolution factor $\mathcal{R}$ is given by

$$\mathcal{R} = \left[\frac{\alpha_s(\bar{m}_h)}{\alpha_s(\bar{m}_b)}\right]^{\frac{\gamma_0}{2\beta_0}} \frac{R(\bar{m}_h)}{R(\bar{m}_b)}, \tag{24}$$

with

$$R(\bar{m}_h) \equiv 1 + r_1 \frac{\alpha_s(\bar{m}_h)}{\pi} + \frac{r_2 + r_1^2}{2}\left(\frac{\alpha_s(\bar{m}_h)}{\pi}\right)^2 \tag{25}$$

and

$$r_1 = \frac{\gamma_0}{2\beta_0}\left(\frac{\gamma_1}{\gamma_0} - \frac{\beta_1}{\beta_0}\right), \qquad r_2 = \frac{\gamma_0}{2\beta_0}\left(\frac{\gamma_2}{\gamma_0} - \frac{\beta_1}{\beta_0}\frac{\gamma_1}{\gamma_0} - \frac{\beta_2}{\beta_0} + \frac{\beta_1^2}{\beta_0^2}\right). \tag{26}$$

In Eq. (26) the parameters β_i and γ_i ($i = 0, 1, 2$) are, respectively, the loop coefficients of the QCD β function and of the anomalous dimension γ_{CMO} of the chromomagnetic operator, namely,

$$\beta_0 = (33 - 2n_\ell)/12, \tag{27}$$

$$\beta_1 = \left(102 - \frac{38}{3}n_\ell\right)\Big/16, \tag{28}$$

$$\beta_2 = \left(2857 - \frac{5033}{9}n_\ell + \frac{325}{27}n_\ell^2\right)\Big/128 \tag{29}$$

and [19]

$$\gamma_0 = \frac{3}{2}, \tag{30}$$

$$\gamma_1 = \left(51 - \frac{13}{2}n_\ell\right)\Big/12, \tag{31}$$

$$\gamma_2 = 27\left(\frac{\zeta_3}{8} + \frac{899}{1728}\right) + \frac{45}{48}\pi^2 - \frac{n_\ell}{4}\left(5\zeta_3 + \frac{57}{6} + \frac{5}{18}\pi^2\right) - \frac{n_\ell^2}{48}. \tag{32}$$

Moreover, from Eq. (12) one has

$$\frac{\tilde{m}_h}{m_h^{\rm pole}} = 1 - \frac{4}{3}\frac{\alpha_s(\bar{m}_h)}{\pi}x\left(\frac{4}{3}+\frac{1}{2}x\right) + \left(\frac{\alpha_s(\bar{m}_h)}{\pi}\right)^2 x\left[\frac{4}{27}(24\beta_0\ln(2x) - 64\beta_0 + 6\pi^2 - 23) + \frac{1}{18}x(24\beta_0\ln(2x) - 52\beta_0 + 6\pi^2 - 7) - \frac{32}{27}x^2 - \frac{4}{9}x^3\right] + \mathcal{O}(\alpha_s^3). \quad (33)$$

Introducing the variable $\tilde{x} \equiv \mu_{\rm soft}/\tilde{m}_h = x\bar{m}_h/\tilde{m}_h$ and taking into account that the values of the coupling constant α_s at the two scales $\bar{m}_h$ and $\tilde{m}_h$ differ by terms of order $\mathcal{O}(\alpha_s^3)$, one finally obtains

$$c_G(\tilde{m}_h,\tilde{m}_b) = \frac{1}{R(\tilde{m}_b)}\left[\frac{\alpha_s(\tilde{m}_h)}{\alpha_s(\tilde{m}_b)}\right]^{\frac{\gamma_0}{2\beta_0}}\left\{1 + \frac{\alpha_s(\tilde{m}_h)}{\pi}\left[\frac{13}{6} - \frac{4}{3}\tilde{x}\left(\frac{4}{3}+\frac{1}{2}\tilde{x}\right) + r_1\right] + \left(\frac{\alpha_s(\tilde{m}_h)}{\pi}\right)^2\left[11.4744\beta_0 - 9.6584 + \frac{r_2+r_1^2}{2} + \frac{13}{6}r_1 + \frac{4}{27}\tilde{x}(24\beta_0\ln(2\tilde{x}) - 64\beta_0 + 6\pi^2 - 65 - 12r_1) + \frac{1}{18}\tilde{x}^2\left(24\beta_0\ln(2\tilde{x}) - 52\beta_0 + 6\pi^2 - \frac{73}{9} - 12r_1\right) - \frac{32}{27}\tilde{x}^3 - \frac{4}{9}\tilde{x}^4\right] + \mathcal{O}(\alpha_s^3)\right\}. \quad (34)$$

The behavior of the coefficient c_G, calculated at orders $\mathcal{O}(\alpha_s)$ and $\mathcal{O}(\alpha_s^2)$, is shown in Fig. 7 in the case of the kinetic and pole-mass schemes, i.e., Eq. (34) with $\tilde{x} \neq 0$ and $\tilde{x} = 0$, respectively. It can be seen that the inclusion of the mass factor $\tilde{m}_h/m_h^{\rm pole}$ in Eq. (22) significantly improves the convergence of the perturbative expansion, in agreement with expectations.

The ratios (20) are extrapolated to the physical pion mass and to the continuum limit using a combined linear fit in both $\bar{m}_\ell$ and a^2, as shown in Fig. 8, obtaining a value which will be denoted hereafter by $\bar{y}_{\Delta M}(\tilde{m}_h^{(n)},\lambda)$.

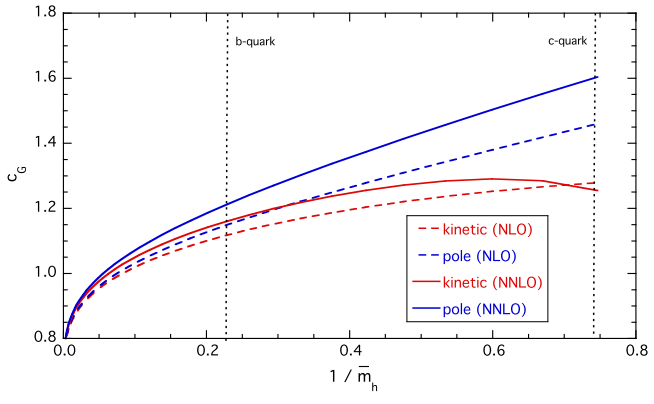

FIG. 7. The Wilson coefficient c_G evaluated at orders $\mathcal{O}(\alpha_s)$ (dashed lines) and $\mathcal{O}(\alpha_s^2)$ (solid lines) in the kinetic scheme (red lines) and in the pole-mass scheme (blue lines), i.e., using Eq. (34) with $\tilde{x} \neq 0$ and $\tilde{x} = 0$, respectively. The vertical dotted lines correspond to the locations of the inverse physical b-quark and c-quark masses.

In the static limit $\tilde{m}_h \to \infty$ the HQE predicts

$$\lim_{\tilde{m}_h\to\infty}\tilde{m}_h\frac{\Delta M(\tilde{m}_h)}{c_G(\tilde{m}_h,\tilde{m}_b)} = \frac{2}{3}\mu_G^2(\tilde{m}_b). \quad (35)$$

The HQE constraint (35) implies $\lim_{\tilde{m}_h\to\infty} y_{\Delta M}(\tilde{m}_h,\lambda) = 1$ for any value of λ. Thus the $\tilde{m}_h$ dependence of $\bar{y}_{\Delta M}$ can be described as a series expansion in terms of $1/\tilde{m}_h$, namely,

$$\bar{y}_{\Delta M}(\tilde{m}_h,\lambda) = 1 + \frac{\Delta\epsilon_1}{\tilde{m}_h} + \frac{\Delta\epsilon_2}{\tilde{m}_h^2} + \mathcal{O}\left(\frac{1}{\tilde{m}_h^3}\right), \quad (36)$$

where the coefficients $\Delta\epsilon_{1,2}$ may depend on λ. The lattice data for the ratio $\bar{y}_{\Delta M}(\tilde{m}_h,\lambda)$ are shown in Fig. 9 as a function of the inverse heavy-quark mass $1/\tilde{m}_h$. Large errors are visible at the heaviest heavy-quark masses at variance with the spin-averaged case (see Fig. 5). This is related to the larger uncertainties affecting the hyperfine quantity ΔM, which becomes smaller as the heavy-quark mass increases, at variance with the case of the spin-averaged quantity M_{av}. As in the case of the spin-averaged ratios, a linear fitting function can be applied to the lattice data, taking into account the correlations between the lattice points for each of the eight branches of the analysis. The quality of the fit (36) with $\Delta\epsilon_2 = 0$ is illustrated in Fig. 9.

Using a chain equation analogous to Eq. (17) but expressed in terms of the ratios (20) and adopting the

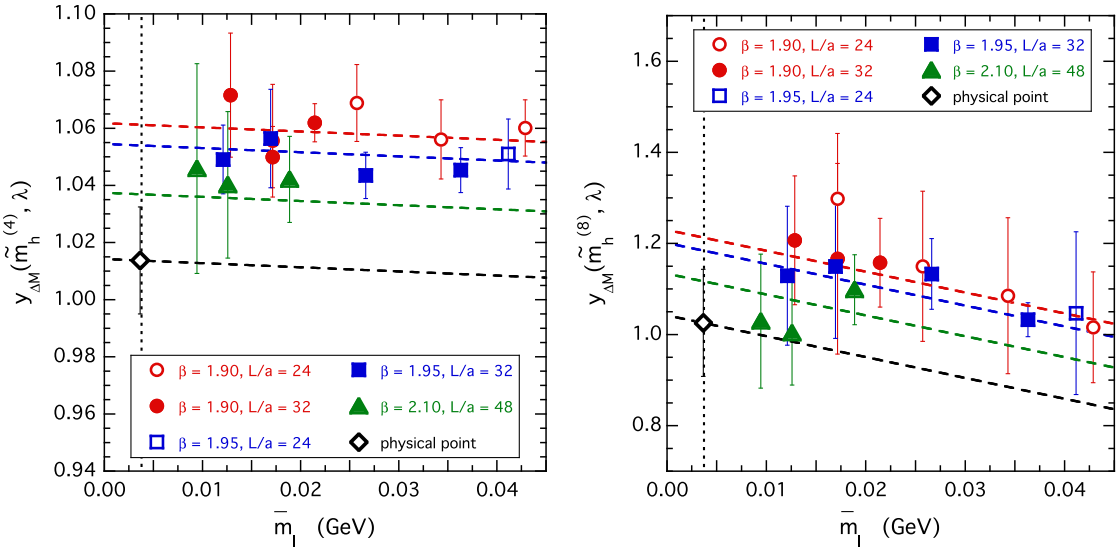

FIG. 8. The ratios $y_{\Delta M}(\tilde{m}_h^{(4)},\lambda)$ (left panel) and $y_{\Delta M}(\tilde{m}_h^{(8)},\lambda)$ (right panel) versus the (renormalized) light-quark mass $\bar{m}_\ell = \bar{m}_\ell(2\ \mathrm{GeV})$ for the various ETMC gauge ensembles. The solid lines are the results of a linear fit in both $\bar{m}_\ell$ and a^2. The black dots correspond to the values $\bar{y}_{\Delta M}(\tilde{m}_h^{(4)},\lambda)$ and $\bar{y}_{\Delta M}(\tilde{m}_h^{(8)},\lambda)$, obtained at the physical light-quark mass m_{ud}^{phys} (see Table II) in the continuum limit.

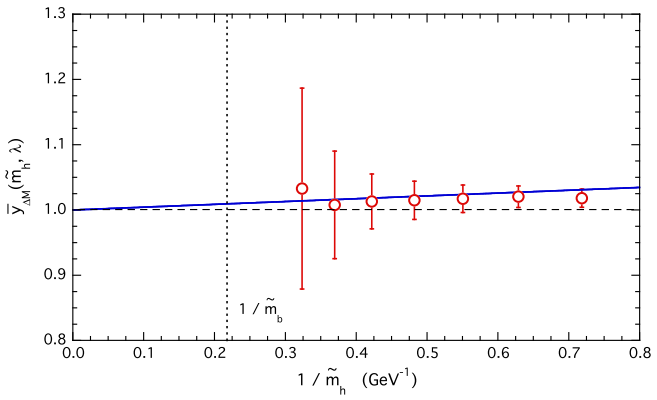

FIG. 9. Lattice data for the ratio $\bar{y}_{\Delta M}(\tilde{m}_h,\lambda)$ versus the inverse heavy-quark mass $1/\tilde{m}_h$. The solid line is the result of the HQE-constrained fit (36) with $\Delta\epsilon_2 = 0$, taking into account the correlation matrix among the lattice points. The vertical dotted line corresponds to the position of the inverse physical b-quark mass $1/\tilde{m}_b$.

values of the parameters λ and K determined in the previous section to reach the physical b-quark mass (18), we get for the hyperfine B-meson mass splitting the result $\Delta M(\tilde{m}_b) = M_{B^*} - M_B = 40.2(2.1)$ MeV, which is slightly below the experimental value $M_{B^*} - M_B = 45.42(26)$ MeV [3], but improves the result $M_{B^*} - M_B = 41.2(7.4)$ MeV of Ref. [41], based on the direct investigation of the V to PS meson mass ratios.

Before closing this section, we stress that throughout this work we have adopted four quark flavors ($n_\ell = 4$) and $\Lambda_{\mathrm{QCD}}^{Nf=4} = 297(8)$ MeV [3] not only below, but also above the physical b-quark mass (18). This is done mainly for consistency with the ETMC gauge ensembles used in this work and with the analyses of Ref. [27], in which all the input parameters of Table II have been determined.

VII. DETERMINATION OF THE HQE EXPANSION PARAMETERS

The chain equation (17), as well as the analogous one in terms of the ratios (20), can be easily extended beyond the physical b-quark point using the fitting functions (16) with $\epsilon_2 = 0$ and (36) with $\Delta\epsilon_2 = 0$. In the case of the spin-averaged meson mass one obtains

$$\frac{M_{av}(\tilde{m}_h^{(n)})}{\tilde{m}_h^{(n)}} = \frac{M_{av}(\tilde{m}_c)}{\tilde{m}_c}\prod_{i=2}^{n}\bar{y}_M(\tilde{m}_h^{(i)},\lambda), = \frac{M_{av}(\tilde{m}_c)}{\tilde{m}_c}\prod_{i=2}^{n}\left[1+\frac{\epsilon_1}{\lambda^{i-1}\tilde{m}_c}\right], \quad (37)$$

where $\tilde{m}_h^{(n)} = \lambda^{n-1}\tilde{m}_c$, while for the hyperfine meson mass splitting one gets

$$\tilde{m}_h^{(n)}\frac{\Delta M(\tilde{m}_h^{(n)})}{c_G(\tilde{m}_h^{(n)},\tilde{m}_b)} = \tilde{m}_c\frac{\Delta M(\tilde{m}_c)}{c_G(\tilde{m}_c,\tilde{m}_b)}\prod_{i=2}^{n}\bar{y}_{\Delta M}(\tilde{m}_h^{(i)},\lambda), = \tilde{m}_c\frac{\Delta M(\tilde{m}_c)}{c_G(\tilde{m}_c,\tilde{m}_b)}\prod_{i=2}^{n}\left[1+\frac{\Delta\epsilon_1}{\lambda^{i-1}\tilde{m}_c}\right]. \quad (38)$$

For values of $n > K+1$, Eqs. (37)–(38) provide V and PS heavy-meson masses beyond the physical b-quark point. In the static limit, Eq. (37) implies

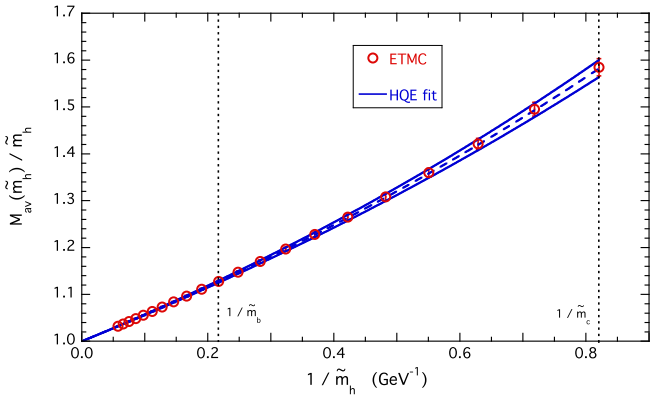

FIG. 10. Lattice data for the quantity $M_{av}(\tilde{m}_h)/\tilde{m}_h$ [Eq. (40)] versus the inverse heavy-quark mass $\tilde{m}_h$. The dashed and solid lines are the results of the HQE fit (41) in which the correlation matrix between the lattice data is taken into account. The dashed line corresponds to the central values of the fits, while the solid lines represent 1 standard deviation. The vertical dotted lines correspond to the positions of the inverse physical b-quark and c-quark masses, $1/\tilde{m}_b$ and $1/\tilde{m}_c$.

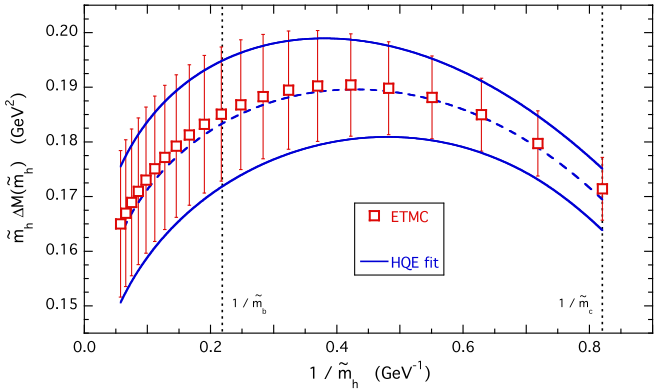

FIG. 11. Lattice data for the quantity $\tilde{m}_h \Delta M(\tilde{m}_h)$ [see Eq. (38)]. The dashed and solid lines are the results of the HQE fit (42), in which the correlation matrix between the lattice data is taken into account. The dashed line corresponds to the central values of the fit, while the solid lines represent 1 standard deviation. The vertical dotted lines correspond to the positions of the inverse physical b-quark and c-quark masses, $1/\tilde{m}_b$ and $1/\tilde{m}_c$, respectively.

$$Z_\infty \equiv \lim_{\tilde{m}_h \to \infty} \frac{M_{av}(\tilde{m}_h)}{\tilde{m}_h} = \frac{M_{av}(\tilde{m}_c)}{\tilde{m}_c} \prod_{i=2}^{\infty} \left[1 + \frac{\epsilon_1}{\lambda^{i-1} \tilde{m}_c} \right]. \tag{39}$$

The HQE predicts that Z_∞ should be equal to unity. Numerically, we find $Z_\infty = 1.023 \pm 0.027$, which is well consistent with unity, but introduces a $\approx 3\%$ uncertainty in the static limit. In order to implement the exact condition $Z_\infty = 1$, for each bootstrap event we divide Eq. (37) by the definition (39), obtaining

$$\frac{M_{av}(\tilde{m}_h^{(n)})}{\tilde{m}_h^{(n)}} = \frac{\prod_{i=2}^{n} [1 + \frac{\epsilon_1}{\lambda^{i-1} \tilde{m}_c}]}{\prod_{i=2}^{\infty} [1 + \frac{\epsilon_1}{\lambda^{i-1} \tilde{m}_c}]}. \tag{40}$$

We have evaluated Eqs. (40) and (38) for $n \lesssim 20$, i.e., for heavy-quark masses up to $\tilde{m}_h \simeq 4\tilde{m}_b$. The results are shown in Figs. 10 and 11. It can be seen that, thanks to the definition (40), the data for the spin-averaged quantity $M_{av}(\tilde{m}_h)/\tilde{m}_h$ are quite precise: the uncertainties are at the level of $\simeq 1\%$ around the charm mass, of $\simeq 0.2\%$ around the bottom mass, and then vanish in the static limit.

Neglecting the effects of dimension-seven operators, the HQE expansion of the heavy-meson masses reads [5]

$$\frac{M_{av}(\tilde{m}_h)}{\tilde{m}_h} = 1 + \frac{\bar{\Lambda}}{\tilde{m}_h} + \frac{\mu_\pi^2}{2\tilde{m}_h^2} + \frac{\rho_D^3 - \rho_{\pi\pi}^3 - \rho_S^3}{4\tilde{m}_h^3}, \tag{41}$$

$$\tilde{m}_h \Delta M(\tilde{m}_h) = \frac{2}{3} c_G(\tilde{m}_h, \tilde{m}_b) \mu_G^2(\tilde{m}_b) + \frac{\rho_{\pi G}^3 + \rho_A^3 - \rho_{LS}^3}{3\tilde{m}_h}, \tag{42}$$

where $\bar{\Lambda}$ is the so-called heavy-quark binding energy, μ_π^2 is the matrix element of the kinetic energy operator, and the parameters ρ_i^3 $(i = D, \pi\pi, S, \pi G, A, LS)$ are the matrix elements of the relevant local and nonlocal operators of dimension six. From now on it is understood that all the HQE parameters appearing in Eqs. (41)–(42) are given in the kinetic scheme at the normalization point $\mu_{\rm soft}$, which is chosen to be equal to 1 GeV.

Taking into account the correlation matrix between the lattice data shown in Figs. 10 and 11, the HQE fits (41) and (42) yield

$$\bar{\Lambda} = 0.551(13)_{\rm stat}(2)_{\rm syst}\ \text{GeV} = 0.551(13)\ \text{GeV}, \tag{43}$$

$$\mu_\pi^2 = 0.314(14)_{\rm stat}(2)_{\rm syst}\ \text{GeV}^2 = 0.314(15)\ \text{GeV}^2, \tag{44}$$

$$\begin{aligned} \rho_D^3 - \rho_{\pi\pi}^3 - \rho_S^3 &= 0.174(12)_{\rm stat}(2)_{\rm syst}\ \text{GeV}^3 \\ &= 0.174(12)\ \text{GeV}^3, \end{aligned} \tag{45}$$

and

$$\mu_G^2(\tilde{m}_b) = 0.250(18)_{\rm stat}(8)_{\rm syst}\ \text{GeV}^2 = 0.250(20)\ \text{GeV}^2, \tag{46}$$

$$\begin{aligned} \rho_{\pi G}^3 + \rho_A^3 - \rho_{LS}^3 &= -0.143(57)_{\rm stat}(21)_{\rm syst}\ \text{GeV}^3 \\ &= -0.143(60)\ \text{GeV}^3. \end{aligned} \tag{47}$$

The quality of the HQE fits is shown in Figs. 10 and 11 by the dashed (central values) and solid (1 standard deviation) lines. We stress the remarkable precision obtained for the determinations of $\bar{\Lambda}$ ($\simeq 2.4\%$), μ_π^2 ($\simeq 4.8\%$), $(\rho_D^3 - \rho_{\pi\pi}^3 - \rho_S^3)$ ($\simeq 6.9\%$), and $\mu_G^2(\tilde{m}_b)$ ($\simeq 8.0\%$), while the quantity $(\rho_{\pi G}^3 + \rho_A^3 - \rho_{LS}^3)$ has a larger uncertainty ($\simeq 42\%$).

The HQE fits (41)–(42) contain all of the terms generated by effective operators up to dimension six, and in what follows we will refer to the fits (41)–(42) as the *"dimension-six"* fit. We have also tried to include the possible contributions arising from operators of dimension seven, which means that a quartic term has to be added to Eq. (41) and a quadratic one to Eq. (42), viz.,

$$\frac{M_{av}(\tilde{m}_h)}{\tilde{m}_h} = 1 + \frac{\bar{\Lambda}}{\tilde{m}_h} + \frac{\mu_\pi^2}{2\tilde{m}_h^2} + \frac{\rho_D^3 - \rho_{\pi\pi}^3 - \rho_S^3}{4\tilde{m}_h^3} + \frac{\sigma^4}{\tilde{m}_h^4}, \quad (48)$$

$$\tilde{m}_h \Delta M(\tilde{m}_h) = \frac{2}{3} c_G(\tilde{m}_h, \tilde{m}_b) \mu_G^2(\tilde{m}_b) + \frac{\rho_{\pi G}^3 + \rho_A^3 - \rho_{LS}^3}{3\tilde{m}_h} + \frac{\Delta\sigma^4}{\tilde{m}_h^2}. \quad (49)$$

We obtain

$$\bar{\Lambda} = 0.552(13)_{\rm stat}(2)_{\rm syst}\ {\rm GeV} = 0.552(13)\ {\rm GeV}, \quad (50)$$

$$\mu_\pi^2 = 0.325(17)_{\rm stat}(3)_{\rm syst}\ {\rm GeV}^2 = 0.325(17)\ {\rm GeV}^2, \quad (51)$$

$$\rho_D^3 - \rho_{\pi\pi}^3 - \rho_S^3 = 0.133(34)_{\rm stat}(6)_{\rm syst}\ {\rm GeV}^3 = 0.133(35)\ {\rm GeV}^3, \quad (52)$$

$$\sigma^4 = 0.0071(55)_{\rm stat}(10)_{\rm syst}\ {\rm GeV}^4 = 0.0071(55)\ {\rm GeV}^4, \quad (53)$$

and

$$\mu_G^2(\tilde{m}_b) = 0.254(20)_{\rm stat}(9)_{\rm syst}\ {\rm GeV}^2 = 0.254(22)\ {\rm GeV}^2, \quad (54)$$

$$\rho_{\pi G}^3 + \rho_A^3 - \rho_{LS}^3 = -0.173(74)_{\rm stat}(25)_{\rm syst}\ {\rm GeV}^3 = -0.173(79)\ {\rm GeV}^3, \quad (55)$$

$$\Delta\sigma^4 = 0.0092(58)_{\rm stat}(14)_{\rm syst}\ {\rm GeV}^4 = 0.0092(60)\ {\rm GeV}^4. \quad (56)$$

It can be seen that the values of the HQE parameters related to operators up to dimension-six are found to be consistent between the *"dimension-six"* and *"dimension-seven"* fits. In particular, the results (50), (51), and (54) of the *"dimension-seven"* fit nicely confirm both the central values and the uncertainties (43), (44), and (46) of the *"dimension-six"* fit. The result (55) is consistent with the corresponding one (45) within a larger uncertainty and, finally, the terms (53) and (56) coming from dimension-seven operators are found to be almost consistent with zero.

We note the following:

(1) Equations (44) and (46) and Eqs. (51) and (54) imply $(\mu_\pi^2 - \mu_G^2) = 0.064(19)\ {\rm GeV}^2$ for the *"dimension-six"* fit and $(\mu_\pi^2 - \mu_G^2) = 0.072(22)\ {\rm GeV}^2$ for the *"dimension-seven"* fit, respectively. These findings represent a deviation from the so-called BPS limit $\mu_\pi^2 = \mu_G^2$ [42]. The deviation is equal to ≈20–25% of the kinetic energy term.

(2) Equations (45) and (47) [Eqs. (52) and (55)] imply $\rho_{\pi\pi}^3 + \rho_S^3 + \rho_{\pi G}^3 + \rho_A^3 = \rho_D^3 + \rho_{LS}^3 - 0.317(65)\ {\rm GeV}^3$ [$0.306(86)\ {\rm GeV}^3$] for the *"dimension-six"* [*"dimension-seven"*] fit. Since the sum $\rho_{\pi\pi}^3 + \rho_S^3 + \rho_{\pi G}^3 + \rho_A^3$ is always positive definite [5], it follows that $\rho_D^3 + \rho_{LS}^3 \geq 0.317(65)\ {\rm GeV}^3$ [$0.306(86)\ {\rm GeV}^3$] for the *"dimension-six"* [*"dimension-seven"*] fit. These results show a very sizable deviation from the BPS limit $\rho_D^3 + \rho_{LS}^3 = 0$ at the level of ≈4.9 (3.6) standard deviations.

The correlations among the b-quark mass and the HQE parameters of the *"dimension-six"* and *"dimension-seven"* fits are summarized in Tables IV and V, respectively. The correlations can easily be taken into account by using our bootstrap samplings, which are available upon request.

From Table IV it can be seen that the spin-averaged parameters $\bar{\Lambda}$, μ_π^2 and $(\rho_D^3 - \rho_{\pi\pi}^3 - \rho_S^3)$ and, separately, the hyperfine ones μ_G^2 and $(\rho_{\pi G}^3 + \rho_A^3 - \rho_{LS}^3)$ are strongly correlated or anticorrelated among themselves. Moreover, since our bootstrap sampling takes into account the correlations between the input parameters of Table II, the data for the spin-averaged meson masses and the hyperfine splitting are partially correlated. This induces a partial correlation among the hyperfine and the spin-averaged parameters. Finally, the b-quark mass $\tilde{m}_b$, and correspondingly also the charm mass $\tilde{m}_c$ [see Eq. (19)], turn out to be strongly correlated with the spin-averaged HQE parameters and only partially with the hyperfine ones. In the case of the *"dimension-seven"* fit the correlations (see Table V) appear to be milder than the corresponding ones of the *"dimension-six"* fit.

As a further consistency check, we have repeated our analysis in the case of the heavy-quark mass dependence of the quantity $M_{\rm V}^2 - M_{\rm PS}^2$, using the experimental value $M_{D^*}^2 - M_D^2$ at the triggering point. The corresponding data are shown in Fig. 12 and the HQE expansion reads [5]

TABLE IV. Correlation matrix among the b-quark mass and the HQE parameters of the *"dimension-six"* fit based on Eqs. (41) and (42). The quantities ρ^3 and $\Delta\rho^3$ stand for $\rho_D^3 - \rho_{\pi\pi}^3 - \rho_S^3$ and $\rho_{\pi G}^3 + \rho_A^3 - \rho_{LS}^3$, respectively.

	$\tilde{m}_b$	$\bar{\Lambda}$	μ_π^2	ρ^3	$\mu_G^2(\tilde{m}_b)$	$\Delta\rho^3$
$\tilde{m}_b$	1.0	0.905	0.910	0.886	0.572	−0.488
$\bar{\Lambda}$	0.905	1.0	0.999	0.999	0.497	−0.420
μ_π^2	0.910	0.999	1.0	−0.998	0.501	−0.423
ρ^3	0.886	0.999	−0.998	1.0	0.484	−0.408
$\mu_G^2(\tilde{m}_b)$	0.572	0.497	0.501	0.484	1.0	−0.995
$\Delta\rho^3$	−0.488	−0.420	−0.423	−0.408	−0.995	1.0

TABLE V. Correlation matrix among the b-quark mass and the HQE parameters of the *"dimension-seven"* fit based on Eqs. (48) and (49). The quantities ρ^3 and $\Delta\rho^3$ stand for $\rho_D^3-\rho_{\pi\pi}^3-\rho_S^3$ and $\rho_{\pi G}^3+\rho_A^3-\rho_{LS}^3$, respectively.

	$\tilde{m}_b$	$\bar{\Lambda}$	μ_π^2	ρ^3	σ^4	$\mu_G^2(\tilde{m}_b)$	$\Delta\rho^3$	$\Delta\sigma^4$
$\tilde{m}_b$	1.0	0.910	0.811	0.394	0.196	0.538	−0.440	0.312
$\bar{\Lambda}$	0.910	1.0	0.886	0.439	0.223	0.466	−0.375	0.260
μ_π^2	0.811	0.886	1.0	0.082	0.568	0.443	−0.362	0.258
ρ^3	0.394	0.439	0.082	1.0	−0.693	0.151	−0.108	0.057
σ^4	0.196	0.223	0.568	−0.693	1.0	0.155	−0.137	0.111
$\mu_G^2(\tilde{m}_b)$	0.538	0.466	0.443	0.151	0.155	1.0	−0.993	0.961
$\Delta\rho^3$	−0.440	−0.375	−0.362	−0.108	−0.37	−0.993	1.0	−0.986
$\Delta\sigma^4$	0.312	0.260	0.258	0.057	0.111	0.961	−0.986	1.0

$$M_{\rm V}^2-M_{\rm PS}^2=\frac{4}{3}c_G(\tilde{m}_h,\tilde{m}_b)\mu_G^2(\tilde{m}_b)+\frac{2}{3}\frac{\rho_{\pi G}^3+\rho_A^3-\rho_{LS}^3+2\bar{\Lambda}\mu_G^2(\tilde{m}_b)}{\tilde{m}_h}+\frac{\Delta\tilde{\rho}^4}{\tilde{m}_h^2}. \tag{57}$$

Taking into account the correlation matrix between the lattice data, the HQE fit (57) (see the solid and dashed lines in Fig. 12) yields

$$\mu_G^2(\tilde{m}_b)=0.270(17)\ \text{GeV}^2, \tag{58}$$

$$\rho_{\pi G}^3+\rho_A^3-\rho_{LS}^3+2\bar{\Lambda}\mu_G^2(\tilde{m}_b)=0.164(46)\ \text{GeV}^3, \tag{59}$$

$$\Delta\tilde{\rho}^4=0.010(8)\ \text{GeV}^4. \tag{60}$$

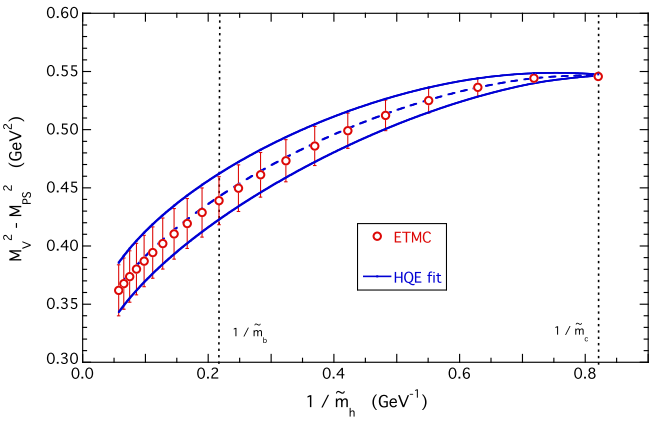

FIG. 12. Lattice data for the quantity $M_{\rm V}^2-M_{\rm PS}^2$ versus the inverse heavy-quark mass $\tilde{m}_h$. The dashed and solid lines are the result of the HQE fit (57), in which the correlation matrix between the lattice data is taken into account. The dashed line corresponds to the central values of the fits, while the solid lines represent 1 standard deviation. The vertical dotted lines correspond to the positions of the inverse physical b-quark and c-quark masses, $1/\tilde{m}_b$ and $1/\tilde{m}_c$. At the charm mass the experimental value and the error from Ref. [3] are adopted.

It can be seen that the result (58) for $\mu_G^2(\tilde{m}_b)$ is consistent with the corresponding one given in Eq. (54). Using the findings (50) for $\bar{\Lambda}$ and (58) for $\mu_G^2(\tilde{m}_b)$, Eq. (59) implies

$$\rho_{\pi G}^3+\rho_A^3-\rho_{LS}^3=-0.134(67)\ \text{GeV}^3, \tag{61}$$

which is compatible with the result (55) within the uncertainties.

The results (43)–(47) and (50)–(56) of the dimension-six and dimension-seven fits have been obtained by including radiative corrections up to order $O(\alpha_s^2)$. Higher-order terms might have an impact on the extraction of the HQE parameters, which are expected to be maximal around the charm mass region. Therefore, we have applied the dimension-six fit (41)–(42) to the lattice data, limiting the range of the heavy-quark masses either to $\tilde{m}_h\geq 2\tilde{m}_c$ or to $\tilde{m}_h\geq\tilde{m}_b$. The corresponding results are shown in Table VI and compared with the ones obtained in the full range of heavy-quark masses $\tilde{m}_h\geq\tilde{m}_c$. It can be seen that the parameters $\bar{\Lambda}$, μ_π^2, and $\mu_G^2(\tilde{m}_b)$ (i.e., the matrix elements of operators up to dimension five) are almost totally insensitive to the range of heavy-quark masses considered, whereas the dimension-six parameters $\rho_D^3-\rho_{\pi\pi}^3-\rho_S^3$ and $\rho_{\pi G}^3+\rho_A^3-\rho_{LS}^3$ are only marginally sensitive to the presence of data in the charm region (i.e., they are consistent within 1 standard deviation).

In order to obtain our final determinations of the HQE parameters we perform the average of the results

TABLE VI. Results obtained for the HQE parameters $\bar{\Lambda}$, μ_π^2, $\rho_D^3-\rho_{\pi\pi}^3-\rho_S^3$, $\mu_G^2(\tilde{m}_b)$, and $\rho_{\pi G}^3+\rho_A^3-\rho_{LS}^3$ for different ranges of the heavy-quark mass $\tilde{m}_h$ included in the *"dimension-six"* fit (41)–(42).

HQE parameter	$\tilde{m}_h\geq\tilde{m}_b$	$\tilde{m}_h\geq 2\tilde{m}_c$	$\tilde{m}_h\geq\tilde{m}_c$
$\bar{\Lambda}$ (GeV)	0.552 (13)	0.552 (13)	0.551 (13)
μ_π^2 (GeV^2)	0.325 (15)	0.323 (16)	0.314 (15)
$\rho_D^3-\rho_{\pi\pi}^3-\rho_S^3$ (GeV^3)	0.146 (31)	0.153 (24)	0.174 (12)
$\mu_G^2(\tilde{m}_b)$ (GeV^2)	0.253 (22)	0.254 (22)	0.250 (20)
$\rho_{\pi G}^3+\rho_A^3-\rho_{LS}^3$ (GeV^3)	−0.133 (69)	−0.158 (70)	−0.143 (60)

corresponding to the *"dimension-six"* and *"dimension-seven"* fits as well as to the *"dimension-six"* fit with the range of the heavy-quark masses limited to $\tilde{m}_h \geq 2\tilde{m}_c$ (see third column of Table VI). The average and the corresponding uncertainty are evaluated according to Eq. (28) of Ref. [27]. Moreover, we want to consider the impact of the uncertainty in the conversion from the $\overline{\text{MS}}$ scheme to the kinetic one at the charm mass on the extracted HQE parameters As a matter of fact, a systematic shift of the value of $\tilde{m}_c$ can propagate into the chain of the heavy-quark masses, leading to a change of the values of the extracted HQE parameters. Thus, we have shifted the value of $\tilde{m}_c$ by 40 MeV [43] and repeated our whole analysis, obtaining a change equal to 0.150 GeV for $\tilde{m}_b$, 0.022 GeV for $\bar{\Lambda}$, 0.027 GeV^2 for μ_π^2, 0.017 GeV^3 for $\rho_D^3 - \rho_{\pi\pi}^3 - \rho_S^3$, 0.013 GeV^2 for $\mu_G^2(m_b)$, and 0.045 GeV^3 for $\rho_{\pi G}^3 + \rho_A^3 - \rho_{LS}^3$.

The inclusion of the above uncertainties (added in quadrature) leads to the final results

$$\tilde{m}_c = 1.219(41)(40)_{\text{conv}}\ \text{GeV} = 1.219(57)\ \text{GeV}, \tag{62}$$

$$\tilde{m}_b = 4.605(132)(150)_{\text{conv}}\ \text{GeV} = 4.605(201)\ \text{GeV}, \tag{63}$$

$$\bar{\Lambda} = 0.552(13)(22)_{\text{conv}}\ \text{GeV} = 0.552(26)\ \text{GeV}, \tag{64}$$

$$\mu_\pi^2 = 0.321(17)(27)_{\text{conv}}\ \text{GeV}^2 = 0.321(32)\ \text{GeV}^2, \tag{65}$$

$$\rho_D^3 - \rho_{\pi\pi}^3 - \rho_S^3 = 0.153(30)(17)_{\text{conv}}\ \text{GeV}^3 = 0.153(34)\ \text{GeV}^3, \tag{66}$$

$$\mu_G^2(m_b) = 0.253(21)(13)_{\text{conv}}\ \text{GeV}^2 = 0.253(25)\ \text{GeV}^2, \tag{67}$$

$$\begin{aligned}\rho_{\pi G}^3 + \rho_A^3 - \rho_{LS}^3 &= -0.158(71)(45)_{\text{conv}}\ \text{GeV}^3 \\ &= -0.158(84)\ \text{GeV}^3,\end{aligned} \tag{68}$$

where $()_{\text{conv}}$ indicates the errors generated by the uncertainty in the conversion from the $\overline{\text{MS}}$ scheme to the kinetic one at the charm mass. The reduction of this source of uncertainty will certainly deserve future investigations.

Before closing this section, we want to briefly comment on the relation between our results and those obtained in recent analyses of the inclusive semileptonic B-meson decays [1,2].

We start by warning the reader that in this work μ_π^2 and $\mu_G^2(m_b)$ refer to asymptotic matrix elements, i.e., matrix elements of asymptotically heavy mesons, while the inclusive semileptonic fits are sensitive to the matrix elements of the same operators in the physical B meson. The relations between the two concepts are

$$\mu_\pi^2|_B = \mu_\pi^2|_\infty - \frac{\rho_{\pi\pi}^3 + \frac{1}{2}\rho_{\pi G}^3}{\tilde{m}_b} + \mathcal{O}(1/\tilde{m}_b^2), \tag{69}$$

$$\mu_G^2(m_b)|_B = \mu_G^2(m_b)|_\infty + \frac{\rho_S^3 + \rho_A^3 + \frac{1}{2}\rho_{\pi G}^3}{\tilde{m}_b} + \mathcal{O}(1/\tilde{m}_b^2). \tag{70}$$

It should also be kept in mind that the semileptonic fits are not very sensitive to $\mu_G^2(m_b)$ and ρ_{LS}^3, which are mostly determined by loose constraints based on heavy-quark sum rules. In particular, the constraint $\mu_G^2(m_b)|_B = 0.35(7)$ GeV^2 was applied in Refs. [1,2]. As a first application of our results we can check their consistency with this constraint. The values $\mu_\pi^2|_B = 0.432(68)$ GeV^2 and $\mu_\pi^2|_B = 0.465(68)$ GeV^2 were found in Refs. [1,2], respectively, which differ only in the inclusion of higher-order power corrections. Comparing these values with our final result (63), it follows that the combination $\rho_{\pi\pi}^3 + \frac{1}{2}\rho_{\pi G}^3$ should be large and negative, $-0.51(35)$ GeV^2, where we have taken the smaller value of $\mu_\pi^2|_B$ from Ref. [1]. Since the sum $\rho_{\pi\pi}^3 + \rho_S^3 + \rho_A^3 + \rho_{\pi G}^3$ is positive by definition, it also follows that $\rho_S^3 + \rho_A^3 + \frac{1}{2}\rho_{\pi G}^3 > 0.51(35)$ GeV^2, or $\mu_G^2|_B > \mu_G^2|_\infty + 0.11(8)$ GeV^2 $= 0.36(8)$ GeV^2. Despite the large errors, there is a clear indication that the constraint employed in the semileptonic fits is adequate. We also note that the large values taken by some of the nonlocal matrix elements are consistent with the observations made in Ref. [5]. A detailed discussion of our results in the context of the heavy-quark sum rules and in particular of the zero-recoil sum rule is postponed to a future publication.

Of course, in order to employ our results in other observables (like the inclusive semileptonic decay rates of the B meson), it is necessary that all of the matrix elements are defined as short-distance quantities, not affected by renormalons. As is well known, the OPE of the inclusive semileptonic B-meson decay rate predicts [44] that the corrections to the free-quark decay rate are suppressed by two powers of the b-quark mass and can be parametrized in terms of the HQE matrix elements μ_π^2 and $\mu_G^2(m_b)$. In terms of the heavy-quark pole mass the radiative corrections to the free-quark decay rate are plagued by renormalons, which however are canceled out when the pole mass is replaced in favor of a short-distance heavy-quark mass [12,45]. This is a crucial feature for the OPE analysis of the inclusive semileptonic B-meson decays, since the appearance of renormalons in the radiative corrections of the leading-order decay rate may signal the presence of nonperturbative corrections in the inverse heavy-quark mass, which cannot be parametrized using the same HQE matrix elements μ_π^2 and $\mu_G^2(m_b)$ extracted from the analysis of heavy-meson masses. In principle, the kinetic scheme is designed to achieve precisely that.

VIII. CONCLUSIONS

We have presented a precise lattice computation of pseudoscalar and vector heavy-light meson masses for heavy-quark masses ranging from the physical charm mass up to $\simeq$4 times the physical b-quark mass, adopting the gauge configurations generated by ETMC with $N_f = 2 + 1 + 1$ dynamical quarks at three values of the lattice spacing ($a \simeq 0.062, 0.082, 0.089$ fm) with pion masses in the range $M_\pi \simeq 210$–450 MeV. The heavy-quark mass has been simulated directly on the lattice up to $\simeq$3 times the physical charm mass. The interpolation to the physical b-quark mass has been performed using the *ETMC ratio* method, based on ratios of the spin-averaged meson masses computed at nearby heavy-quark masses.

The kinetic mass scheme has been adopted in order to work with a short-distance mass free from renormalon ambiguities (which is also often used in the analysis of the inclusive semileptonic B-meson decays relevant for the determination of the CKM entry V_{cb}). The extrapolation to the physical pion mass and to the continuum limit yields $m_b^{\rm kin}(1\ {\rm GeV}) = 4.61(20)$ GeV, which corresponds to $\bar{m}_b(\bar{m}_b) = 4.26(18)$ GeV in the $\overline{\rm MS}$ scheme, and is in agreement with the results of the OPE analysis of the inclusive semileptonic B-meson decays [1,2].

Then, the *ratio* method was applied above the physical b-quark mass to provide heavy-light meson masses towards the static point. The lattice data were analyzed in terms of the heavy-quark expansion and the matrix elements of dimension-four and dimension-five operators were determined with a good precision, namely,

$$\bar{\Lambda} = 0.552(26)\ {\rm GeV}, \tag{71}$$

$$\mu_\pi^2 = 0.321(32)\ {\rm GeV}^2, \tag{72}$$

$$\mu_G^2(m_b) = 0.253(25)\ {\rm GeV}^2. \tag{73}$$

The data has also allowed to estimate the size of two combinations of the matrix elements of dimension-six operators, namely,

$$\rho_D^3 - \rho_{\pi\pi}^3 - \rho_S^3 = 0.153(34)\ {\rm GeV}^3, \tag{74}$$

$$\rho_{\pi G}^3 + \rho_A^3 - \rho_{LS}^3 = -0.158(84)\ {\rm GeV}^3. \tag{75}$$

All of the above HQE parameters, as well as the physical c- and b-quark masses, were found to be highly correlated and therefore the full covariance matrix has been provided (see Tables IV–V). We stress that our results (71)–(75), which are specific to the kinetic scheme, represent the first unquenched lattice determinations of the HQE parameters.

The extracted dimension-five and dimension-six HQE parameters play an important role in the OPE analysis of the inclusive semileptonic B-meson decays relevant for the determination of the CKM entries V_{ub} and V_{cb}. Combining our lattice QCD findings with the results of recent analyses of inclusive semileptonic decays, we have been able to test the value of the chromomagnetic matrix element that is currently employed in the inclusive semileptonic fits, which provide to date the most precise determination of $|V_{cb}|$. Our results can also be used as additional constraints in these fits. Another interesting future application concerns the heavy-quark sum rules which constrain the form factor entering the semileptonic decay $B \to D^* \ell \nu$ at zero recoil; here, the nonlocal correlators $\rho_{A,S,\pi\pi,\pi G}$ play an important role (see Ref. [5]).

ACKNOWLEDGMENTS

We warmly thank P. Dimopoulos, R. Frezzotti, V. Lubicz, G. Martinelli, and C. Tarantino for fruitful discussions and their continuous support. We thank the ETMC members for having generated the gauge configurations used for this study. We gratefully acknowledge the CPU time provided by partnership for advanced computing in Europe (PRACE) under the project PRA067 *"First Lattice QCD study of B-physics with four flavors of dynamical quarks"* and by CINECA under the specific initiative INFN-LQCD123 on the BG/Q system Fermi at CINECA (Italy).

[1] P. Gambino, K. J. Healey, and S. Turczyk, Phys. Lett. B **763**, 60 (2016).
[2] A. Alberti, P. Gambino, K. J. Healey, and S. Nandi, Phys. Rev. Lett. **114**, 061802 (2015).
[3] C. Patrignani *et al.* (Particle Data Group Collaboration), Chin. Phys. C **40**, 100001 (2016).
[4] D. Bigi, P. Gambino, and S. Schacht, Phys. Lett. B **769**, 441 (2017).
[5] P. Gambino, T. Mannel, and N. Uraltsev, J. High Energy Phys. 10 (2012) 169.
[6] B. Blossier *et al.* (ETM Collaboration), J. High Energy Phys. 04 (2010) 049.
[7] P. Dimopoulos *et al.* (ETM Collaboration), J. High Energy Phys. 01 (2012) 046.
[8] N. Carrasco *et al.* (ETM Collaboration), J. High Energy Phys. 03 (2014) 016.
[9] A. Bussone *et al.* (ETM Collaboration), Phys. Rev. D **93**, 114505 (2016).
[10] I. I. Y. Bigi, M. A. Shifman, N. G. Uraltsev, and A. I. Vainshtein, Phys. Rev. D **50**, 2234 (1994).

[11] I. I. Y. Bigi, M. A. Shifman, N. Uraltsev, and A. I. Vainshtein, Phys. Rev. D **56**, 4017 (1997).
[12] M. Beneke and V. M. Braun, Nucl. Phys. **B426**, 301 (1994).
[13] M. E. Luke, A. V. Manohar, and M. J. Savage, Phys. Rev. D **51**, 4924 (1995).
[14] G. Martinelli and C. T. Sachrajda, Phys. Lett. B **354**, 423 (1995).
[15] P. Gambino, J. High Energy Phys. 09 (2011) 055.
[16] S. Aoki *et al.*, Eur. Phys. J. C **77**, 112 (2017).
[17] J. Heitger, A. Juttner, R. Sommer, and J. Wennekers (ALPHA Collaboration), J. High Energy Phys. 11 (2004) 048.
[18] D. Guazzini, R. Sommer, and H. Meyer (ALPHA Collaboration), J. High Energy Phys. 10 (2007) 081.
[19] A. G. Grozin, P. Marquard, J. H. Piclum, and M. Steinhauser, Nucl. Phys. **B789**, 277 (2008).
[20] A. K. Ewing, J. M. Flynn, C. T. Sachrajda, N. Stella, H. Wittig, K. C. Bowler, R. D. Kenway, J. Mehegan, D. G. Richards, and C. Michael (UKQCD Collaboration), Phys. Rev. D **54**, 3526 (1996).
[21] V. Gimenez, G. Martinelli, and C. T. Sachrajda, Phys. Lett. B **393**, 124 (1997).
[22] V. Gimenez, G. Martinelli, and C. T. Sachrajda, Nucl. Phys. **B486**, 227 (1997).
[23] A. S. Kronfeld and J. N. Simone, Phys. Lett. B **490**, 228 (2000); **495**, 441(E) (2000).
[24] J. Komijani *et al.*, *Proc. Sci.*, LATTICE2016 (2016) 294, arXiv:1611.07411.
[25] R. Baron *et al.* (ETM Collaboration), J. High Energy Phys. 06 (2010) 111.
[26] R. Baron *et al.* (ETM Collaboration), *Proc. Sci.*, LATTICE2010 (2010) 123, arXiv:1101.0518.
[27] N. Carrasco *et al.* (ETM Collaboration), Nucl. Phys. **B887**, 19 (2014).
[28] Y. Iwasaki, Nucl. Phys. **B258**, 141 (1985).
[29] R. Frezzotti *et al.* (Alpha Collaboration), J. High Energy Phys. 08 (2001) 058.
[30] R. Frezzotti and G. C. Rossi, Nucl. Phys. B, Proc. Suppl. **128**, 193 (2004).
[31] R. Frezzotti and G. C. Rossi, J. High Energy Phys. 08 (2004) 007.
[32] K. Osterwalder and E. Seiler, Ann. Phys. (N.Y.) **110**, 440 (1978).
[33] R. Frezzotti and G. C. Rossi, J. High Energy Phys. 10 (2004) 070.
[34] M. Foster, and C. Michael (UKQCD Collaboration), Phys. Rev. D **59**, 074503 (1999).
[35] C. McNeile, and C. Michael (UKQCD Collaboration), Phys. Rev. D **73**, 074506 (2006).
[36] S. Gusken, Nucl. Phys. B, Proc. Suppl. **17**, 361 (1990).
[37] M. Albanese *et al.* (APE Collaboration), Phys. Lett. B **192**, 163 (1987).
[38] B. Blossier, M. Della Morte, G. von Hippel, T. Mendes,, and R. Sommer, J. High Energy Phys. 04 (2009) 094.
[39] A. Czarnecki, K. Melnikov, and N. Uraltsev, Phys. Rev. Lett. **80**, 3189 (1998).
[40] K. G. Chetyrkin and A. Retey, Nucl. Phys. **B583**, 3 (2000).
[41] V. Lubicz, A. Melis, and S. Simula, *Proc. Sci.*, LATTICE2016 (2016) 291, arXiv:1610.09671.
[42] N. Uraltsev, Phys. Lett. B **585**, 253 (2004).
[43] In Ref. [15], the uncertainty in the conversion from $\bar{m}_c(\bar{m}_c)$ to $\tilde{m}_c$ was estimated to be ≈20 MeV. We have conservatively doubled that uncertainty.
[44] J. Chay, H. Georgi, and B. Grinstein, Phys. Lett. B **247**, 399 (1990); I. I. Y. Bigi, N. G. Uraltsev, and A. I. Vainshtein, Phys. Lett. B **293**, 430 (1992); **297**, 477(E) (1992); I. I. Y. Bigi, M. A. Shifman, N. G. Uraltsev, and A. I. Vainshtein, Phys. Rev. Lett. **71**, 496 (1993).
[45] M. Beneke, V. M. Braun, and V. I. Zakharov, Phys. Rev. Lett. **73**, 3058 (1994).